

protein by $\text{Fe}(\text{EDTA})^{2-4a}$ with eq 4 and find that about 30% of the pH dependence of this reaction results from the pH dependence of the thermodynamic driving force.

The similarity of the results reported here for the ionic strength dependences of the reduction potential and $\text{Fe}(\text{EDTA})^{2-}$ reduction kinetics with those previously observed for the native protein^{4a} is not altogether surprising insofar as the heme vinyl groups are located in the interior of the heme binding pocket of the cytochrome. In this location they would not be expected to contribute appreciably to the apparent surface properties of the protein. In combination, the results obtained from both the ionic strength dependence analysis, the pH dependence analysis, and the Marcus calculations for the $\text{Fe}(\text{EDTA})^{2-}$ reduction kinetics of the native and deuterioheme-substituted cytochrome establish the identity of reaction mechanism that each employs in its reaction with this

and presumably with other small molecule oxidation–reduction reagents.

Acknowledgment. We thank Dr. Bernard Santarsiero for assistance in the use of the software employed in calculation of the angles reported in Table I and for helpful discussions. We also thank Drs. Thomas L. Poulos and Barry Finzel for communicating the coordinates of the heme groups in cytochrome P-450-cam and in the refined structure of cytochrome *c* peroxidase. This research was supported by an operating Grant (MT-7182) from the Medical Research Council of Canada.

Supplementary Material Available: Listing of reduction potentials, Nernst slopes, and observed first-order rate constants (3 pages). Ordering information is given on any current masthead page.

Magnetic Exchange Interactions in Nitroxyl Biradicals Bridged by Metal–Metal Bonded Complexes: Structural, Magnetochemical, and Electronic Spectral Characterization of Tetrakis(perfluorocarboxylato)dimetal(II) Complexes of Rhodium and Molybdenum Containing Axially Coordinated Nitroxyl Radicals

Timothy R. Felthouse,*^{1a} Teng-Yuan Dong,^{1b} David N. Hendrickson,*^{1b}
Huey-Sheng Shieh,^{1a} and Michael R. Thompson^{1a}

Contribution from the School of Chemical Sciences, University of Illinois, Urbana, Illinois 61801, and the Central Research Laboratories, Monsanto Company, St. Louis, Missouri 63167. Received June 12, 1986

Abstract: A series of oxygen-bonded nitroxyl biradicals bridged by $\text{M}_2(\text{O}_2\text{CR})_4$ complexes has been prepared in order to gauge the ability of the metal–metal bonded $\text{M}_2(\text{O}_2\text{C})_4$ cores to propagate a magnetic exchange interaction. The compounds have the general formula $\text{M}_2(\text{O}_2\text{CR})_4(\text{Tempo})_2$, where $\text{M} = \text{Rh}$, $\text{R} = \text{CF}_3$ (**1**); $\text{M} = \text{Rh}$, $\text{R} = \text{C}_3\text{F}_7$ (**2**); $\text{M} = \text{Rh}$, $\text{R} = \text{C}_6\text{F}_5$ (**3**); $\text{M} = \text{Mo}$, $\text{R} = \text{CF}_3$ (**4**); and Tempo is 2,2,6,6-tetramethylpiperidiny-1-oxy. Dark green crystals of **1** and **2** were isolated from toluene solutions and the structures determined by single-crystal X-ray diffraction techniques. Crystallographic data are as follows: **1** (295 K), space group $P\bar{1}$; $a = 8.715$ (2) Å, $b = 10.765$ (3) Å, $c = 11.501$ (3) Å; $\alpha = 107.18$ (2)°, $\beta = 103.30$ (2)°, $\gamma = 107.61$ (2)°; $Z = 1$; $R_1 = 0.0355$; $R_2 = 0.0442$ for 2479 Cu $K\alpha$ data with $I > 2.33\sigma(I)$. **2** (143 K), space group $P2_1/c$; $a = 11.450$ (2) Å, $b = 16.604$ (3) Å, $c = 13.163$ (2) Å; $\beta = 90.30$ (1)°; $Z = 2$; $R_1 = 0.0614$, $R_2 = 0.0669$ for 3409 Mo $K\alpha$ data with $I > 3.00\sigma(I)$. Both structures **1** and **2** consist of typical $\text{Rh}_2(\text{O}_2\text{CR})_4$ frameworks having Rh–Rh bond lengths of 2.417 (1) and 2.431 (1) Å, respectively, while these centrosymmetric structures contain axial O-bonded Tempo ligands with Rh–O distances of 2.220 (2) and 2.234 (5) Å. Variable-temperature (~40–350 K) magnetic susceptibility data for **1–3** reveal the presence of unexpectedly strong antiferromagnetic exchange interactions in these compounds. Least-squares fitting of the χ_M data to the Bleaney–Bowers equation ($S_1 = S_2 = 1/2$ with the isotropic exchange Hamiltonian $-2J\hat{S}_1\hat{S}_2$) produces exchange parameters J of -239 , -269 , and -184 cm^{-1} for **1**, **2**, and **3**, respectively. Variable-temperature (4.2–300 K) magnetic susceptibility data were also obtained for $\text{Mo}_2(\text{O}_2\text{CCF}_3)_4(\text{Tempo})_2$ (**4**) and $\text{Rh}_2(\text{O}_2\text{CCF}_3)_4(\text{Tempo})_2$ (**5**), where Tempo is 4-hydroxy-2,2,6,6-tetramethylpiperidiny-1-oxy. The χ_M data for **4** and **5** follow the Curie–Weiss law throughout the entire temperature range. Electronic absorption and EPR spectral data are also reported for **1–5**. Analysis of the crystal packing geometries in **1** and **2** reveals that the shortest intermolecular nitroxyl group contact distances increase from 4.7 Å in **1** to >6.1 Å in **2** largely as a consequence of the bulkier C_3F_7 groups in **2**. Closely similar singlet–triplet separations in **1** and **2** in conjunction with the lack of any observable magnetic exchange interaction in **4** and **5** suggest that the exchange interactions result from an intramolecular through bond coupling mechanism across the $\text{Rh}_2(\text{O}_2\text{C})_4$ cores despite the more than 6.8-Å separation between radical centers. A discussion is presented on the molecular orbital interactions that lead to efficient spin coupling across the singly bonded $\text{Rh}_2(\text{O}_2\text{C})_4$ framework but produce no observable exchange interaction between nitroxyl groups when bridged by the quadruply bonded $\text{Mo}_2(\text{O}_2\text{C})_4$ core. An $\text{Rh}_2\pi^*-(\text{Tempo})_2\pi^*$ back-bonding model accounts for the strong spin coupling in the $\text{Rh}_2(\text{O}_2\text{CR})_4(\text{Tempo})_2$ compounds, and it is the absence of this $\text{M}_2\pi^*$ back-bonding interaction in $\text{Mo}_2(\text{O}_2\text{CCF}_3)_4(\text{Tempo})_2$ that leads to no spin pairing in this compound. The magnitudes of the intramolecular exchange interactions in the dirhodium–biradical compounds argue against a simple distance-dependence limit function that determines the singlet–triplet separations.

Shortly after the synthesis and characterization of the first nitroxyl biradicals,^{2–5} subsequent investigations discovered a

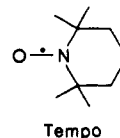
complex relationship between the ground-state singlet–triplet separations in these biradicals and the identity, number, and

conformational mobility of the bridging atoms.⁶⁻⁹ Although the magnetic exchange interaction as gauged by the exchange parameter J was quite small ($|J| < 0.2 \text{ cm}^{-1}$) in these nitroxyl biradicals, analysis of the solution EPR spectra readily afforded the J values. The extreme sensitivity of the exchange parameter to the local environment of the biradical has suggested triplet-state spin probe applications in various biological systems.^{10,11}

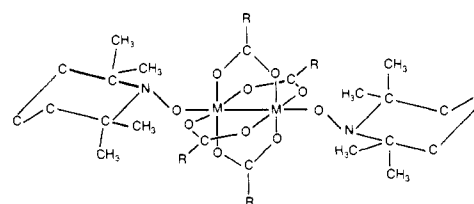
Just as nitroxyl biradicals as well as nitroxyl radicals¹² have been applied as molecular reporter groups of biological macromolecular environments, nitroxyl spin labels have been employed to probe interaction pathways with molecular metal ion complexes.¹³⁻¹⁵ The nitroxyl group has been attached to ligands on the metal ion complex,¹³⁻¹⁵ or the nitroxyl group can function as a Lewis base and coordinate directly to the metal ion.¹⁶ In nearly all of the studies to date involving the interaction between a paramagnetic metal ion and a nitroxyl radical¹³⁻¹⁶ or two nitroxyl radicals,¹⁷ the metal ions are found in mononuclear coordination geometries where no bonding interaction between the metal atoms occurs. Since the recognition over 20 years ago of direct metal-to-metal bonds formed by overlaps of the metal d orbitals,¹⁸ a large class of dinuclear cluster complexes has emerged. While such cluster species have been subjected to extensive chemical and theoretical studies on reactivity and bonding,^{19,20} investigations are lacking toward a determination of the ability of these electron-rich dimetal cores to provide pathways for through bond coupling of unpaired spin density. Thus, two nitroxyl radicals with unpaired electrons in primarily antibonding π^* orbitals²¹ can coordinate through lone pairs on the oxygen atoms to each of two metal atoms comprising a metal-metal bonded unit to produce a biradical complex. The impetus for these studies stems not only from the potential of these biradical cluster species to propagate exchange interactions over multiatomic bridging networks²² but

also for insights into the ground-state electronic structure of these dinuclear (and by analogy, polynuclear) clusters.

As an entry point for the construction of coordinated biradical cluster complexes, the stable nitroxyl free radical 2,2,6,6-tetramethylpiperidinyl-1-oxy (Tempo) was selected since it is devoid of atoms containing lone pairs of electrons other than those of



the nitroxyl group itself. A series of compounds **1-4** has been prepared having the general formula $M_2(O_2CR)_4(\text{Tempo})_2$ and shown schematically below. The tetrakis(carboxylato) complexes of singly bonded dirhodium(II)^{23,24} and quadruply bonded dimolybdenum(II)¹⁹ are well-known to form adducts with trans geometries to the metal-metal bonds. The perfluorinated carboxylate derivatives afford more stable oxygen-bonded adducts with the weak nitroxyl ligands through enhancement of the Lewis acidity of the metal ions.^{16,25,26} Reported herein are the structures of compounds **1** and **2** as determined from single-crystal X-ray diffraction methods, variable-temperature (4.2–350 K) magnetic susceptibility data for **1-4**, and results from electronic absorption



1. M = Rh, R = CF₃
2. M = Rh, R = C₂F₅
3. M = Rh, R = C₆F₅
4. M = Mo, R = CF₃

and EPR spectroscopies. Additionally, magnetic and electronic data are given for $\text{Rh}_2(\text{O}_2\text{CCF}_3)_4(\text{Tempo})_2$ (**5**), where Tempo is 4-hydroxy-2,2,6,6-tetramethylpiperidinyl-1-oxy. The structure of **5** has been previously determined²⁷ and provides an example of a similar type of biradical complex in which the nitroxyl groups are *not* coordinated to the Rh atoms. The exchange interactions observed in these biradical cluster complexes are shown to arise from a through bond coupling mechanism that depends strikingly on the orbital interface between the magnetic orbitals of the nitroxyl radicals and the filled orbitals of the metal-metal bonded complex. Portions of this work have been previously reported.^{22,28,29}

Experimental Section

Compound Preparations. Samples of rhodium(II) acetate³⁰ and molybdenum(II) acetate³¹ were obtained by using published procedures. The perfluorinated carboxylic acids were used as received. The nitroxyl free radicals (Tempo or Tempol) were obtained from Sigma. Because of the low melting point (36–38 °C) of Tempo, it was convenient to

- (1) (a) Monsanto Company. (b) University of Illinois.
- (2) Dupeyre, R. M.; Lemaire, H.; Rassat, A. *J. Am. Chem. Soc.* **1965**, *87*, 3771–3772.
- (3) Brière, R.; Dupeyre, R.-M.; Lemaire, H.; Morat, C.; Rassat, A.; Rey, P. *Bull. Soc. Chim. Fr.* **1965**, 3290–3297.
- (4) Rozantsev, E. G.; Golubev, V. A.; Neiman, M. B. *Izv. Akad. Nauk SSSR, Ser. Khim.* **1965**, 393–394; *Bull. Acad. Sci. USSR, Div. Chem. Sci. (Engl. Transl.)* **1965**, 382–383.
- (5) Rozantsev, E. G.; Golubev, V. A.; Neiman, M. B.; Kokhanov, Yu. V. *Izv. Akad. Nauk SSSR, Ser. Khim.* **1965**, 572–573; *Bull. Acad. Sci. USSR, Div. Chem. Sci. (Engl. Transl.)* **1965**, 559–560.
- (6) Glarum, S. H.; Marshall, J. H. *J. Chem. Phys.* **1967**, *47*, 1374–1378.
- (7) Lemaire, H. *J. Chim. Phys.* **1967**, *64*, 559–571.
- (8) Kokorin, A. I.; Parmon, V. N.; Suskina, V. I.; Ivanov, Yu. A.; Rozantsev, E. G.; Zamarayev, K. I. *Zh. Fiz. Khim.* **1974**, *48*, 953–956; *Russ. J. Phys. Chem. (Engl. Transl.)* **1974**, 548–550.
- (9) Metzner, E. K.; Libertini, L. J.; Calvin, M. *J. Am. Chem. Soc.* **1974**, *96*, 6515–6516.
- (10) Luckhurst, G. R. In *Spin Labeling*; Berliner, L. J., Ed.; Academic: New York, 1976; pp 133–181.
- (11) Parmon, V. N.; Kokorin, A. I.; Zhidomirov, G. M. *Zh. Strukt. Khim.* **1977**, *18*, 132–177; *J. Struct. Chem. (Engl. Transl.)* **1977**, *18*, 104–147.
- (12) Humphries, G. M. K.; McConnell, H. M. *Meth. Expt. Phys.* **1982**, *20*, 53–122.
- (13) Eaton, S. S.; Eaton, G. R. *Coord. Chem. Rev.* **1978**, *26*, 207–262.
- (14) Milaeva, E. R.; Rubezhov, A. Z.; Prokof'ev, A. I.; Okhlobystin, O. Yu. *Usp. Khim.* **1982**, *51*, 1638–1673; *Russ. Chem. Rev. (Engl. Transl.)* **1982**, *51*, 942–960.
- (15) Larionov, S. V. *Zh. Strukt. Khim.* **1982**, *23*, 125–147; *J. Struct. Chem. (Engl. Transl.)* **1982**, *23*, 594–617.
- (16) Porter, L. C.; Dickman, M. H.; Doedens, R. *J. Inorg. Chem.* **1986**, *25*, 678–684 and references therein.
- (17) Intramolecular exchange interactions in di- μ -halo-bridged Pd dimers are known where the nitroxyl groups reside on ligands attached to different Pd atoms: Kokorin, A. I.; Parmon, V. N.; Ovcharenko, V. I.; Larionov, S. V.; Volodarskii, L. B. *Izv. Akad. Nauk SSSR, Ser. Khim.* **1981**, 1763–1768; *Bull. Acad. Sci. USSR, Div. Chem. Sci. (Engl. Transl.)* **1982**, 1433–1437.
- (18) Cotton, F. A.; Curtis, N. F.; Harris, C. B.; Johnson, B. F. G.; Lippard, S. J.; Mague, J. T.; Robinson, W. T.; Wood, J. S. *Science* **1964**, *145*, 1305–1307.
- (19) Cotton, F. A.; Walton, R. A. *Multiple Bonds Between Metal Atoms*; Wiley: New York, 1982.
- (20) Cotton, F. A.; Walton, R. A. *Struct. Bonding (Berlin)* **1985**, *62*, 1–49.
- (21) Morishima, I.; Yoshikawa, K.; Yonekawa, T.; Matsumoto, H. *Chem. Phys. Lett.* **1972**, 336–339.

- (22) Hendrickson, D. N. *NATO ASI SER., SER. C* **1985**, *140*, 523–554.
- (23) Felthouse, T. R. *Prog. Inorg. Chem.* **1982**, *29*, 73–166.
- (24) Boyar, E. B.; Robinson, S. D. *Coord. Chem. Rev.* **1983**, *50*, 109–208.
- (25) Richman, R. M.; Kuechler, T. C.; Tanner, S. P.; Drago, R. S. *J. Am. Chem. Soc.* **1977**, *99*, 1055–1058.
- (26) Bilgrien, C. L.; Drago, R. S.; Stahlbush, J. R.; Kuechler, T. C. *Inorg. Chem.* **1985**, *24*, 4268–4272.
- (27) Cotton, F. A.; Felthouse, T. R. *Inorg. Chem.* **1982**, *21*, 2667–2675.
- (28) Felthouse, T. R.; Shieh, H.-S.; Dong, T.-Y.; Hendrickson, D. N. *Abstracts of Papers*, 187th National Meeting of the American Chemical Society, St. Louis, MO; American Chemical Society: Washington, DC 1984; INOR 77.
- (29) Dong, T.-Y.; Hendrickson, D. N.; Felthouse, T. R.; Shieh, H.-S. *J. Am. Chem. Soc.* **1984**, *106*, 5373–5375.
- (30) Rempel, G. A.; Legzdins, P.; Smith, H.; Wilkinson, G. *Inorg. Synth.* **1972**, *13*, 90–91.
- (31) Stephenson, T. A.; Bannister, E.; Wilkinson, G. *J. Chem. Soc.* **1964**, 2538–2541.

sublime this compound before use under vacuum onto a dry ice cooled cold finger. Solvents were dried before use, and all synthetic manipulations were conducted under an atmosphere of dry argon or nitrogen. Once formed, the dirhodium(II) compounds are air-stable while the dimolybdenum(II) compounds were always maintained under an inert gas atmosphere.

Rh₂(O₂CCF₃)₄(Tempo)₂ (1). Rhodium(II) trifluoroacetate was prepared through a carboxylate exchange procedure³² with rhodium(II) acetate. To a Schlenk flask containing 0.90 g (1.37 mmol) of Rh₂(O₂CCF₃)₄ was added a 30-mL solution of 0.47 g (3.00 mmol, a 10% excess) of Tempo in toluene. The mixture was warmed to 60–70 °C, filtered, and concentrated with cooling to yield a green-black crystalline solid which was recovered by filtration and rinsed with hexanes (10 mL). Yield: 0.71 g (53%). Slow cooling of the filtered toluene solution produced dark green-black crystals suitable for X-ray diffraction studies.

Rh₂(O₂CC₆F₇)₄(Tempo)₂ (2). By using a similar procedure to that described above for **1**, 0.40 g of **2** were isolated from a toluene–hexanes mixture (20% yield) from 1.56 g (1.47 mmol) of Rh₂(O₂CC₆F₇)₄ and 0.51 g (3.26 mmol) of Tempo. Slow concentration and cooling of the toluene–hexanes mixture typically gave large prismatic green-black crystals of **2**, one of which measured 3 × 5 × 7 mm and was used to cut specimens for single-crystal X-ray diffraction analysis (vide infra).

Rh₂(O₂CC₆F₅)₄(Tempo)₂ (3). Samples of Rh₂(O₂CC₆F₅)₄ were obtained from a "melt" exchange of Rh₂(O₂CCH₃)₄, 1.00 g (2.26 mmol), in 5.00 g (23.6 mmol) of pentafluorobenzoic acid at 185 °C for about 1 h followed by a sublimation under vacuum at 150 °C. The crude Rh₂(O₂CC₆F₅)₄ was subjected to a second fusion with C₆F₅CO₂H followed by three vacuum sublimations to remove acetic acid or C₆F₅CO₂H to yield a total of 2.01 g of green Rh₂(O₂CC₆F₅)₄ (yield 87%). To a flask containing 1.00 g of Rh₂(O₂CC₆F₅)₄ (0.98 mmol) was added a 30-mL solution of 0.31 g (0.198 mmol) of Tempo in toluene. The mixture was warmed to about 70 °C and then filtered. Workup of the filtrate yielded two crops of green product, **3**, giving a total of 0.67 g (51%).

Mo₂(O₂CCF₃)₄(Tempo)₂ (4). Molybdenum(II) trifluoroacetate was prepared as described by Cotton and Norman.³³ To a dry benzene solution of Mo₂(O₂CCF₃)₄ (0.40 g, 0.62 mmol) containing Tempo (0.30 g, 1.92 mmol) was added dry *n*-decane to produce an orange powder which was filtered and washed with *n*-decane. Anal. Calcd for **4**: C, 32.65; H, 3.79; N, 2.93. Found: C, 32.36; H, 3.70; N, 3.01.

Rh₂(O₂CCF₃)₄(Tempo)₂ (5).²⁷ For magnetic measurements (vide infra) a light blue solid of this compound was prepared by mixing a toluene solution of Rh₂(O₂CCF₃)₄ (0.54 g, 0.82 mmol) with a toluene solution of Tempo (0.35 g, 2.09 mmol). After the mixture was stirred overnight under nitrogen, the solid was filtered off in air to give 0.80 g (0.80 mmol, 98%) of **5** after being rinsed well with toluene and hexanes and drying in air.

Physical Measurements. Variable-temperature magnetic susceptibility data were acquired on compounds **1–5** with use of a series 800 VTS-50 SQUID susceptometer (S.H.E. Corp.) maintained by the Physics Department at the University of Illinois. The susceptometer was operated at a magnetic field strength of 13 kG for all compounds. Diamagnetic corrections were estimated from Pascal's constants and applied to the calculated molar paramagnetic susceptibilities for compounds **4** and **5**. For compounds **1–3**, the size of the exchange interaction (vide infra) leads to relatively small molar paramagnetic susceptibilities, and so the following procedure was adopted to estimate the temperature-independent paramagnetism (TIP) and diamagnetism in these compounds. A sample of Rh₂(O₂CC₃F₇)₄ was used to obtain magnetic susceptibility data as a function of temperature. From these measurements, a relatively constant value of 3.00835 × 10⁻⁴ cgsu was obtained for the TIP and diamagnetic corrections to **1–3**. This value was then subtracted from the χ_M data at all temperatures for **1–3**.

Electronic absorption spectra were obtained on compounds **1–5**, Rh₂(O₂CC₃F₇)₄, and Tempo by dispersing weighed amounts in KBr and pressing the mixture into a 13-mm pellet. Spectra were recorded on a Varian Model 2300 spectrophotometer at ambient temperatures.

Electron paramagnetic resonance (EPR) spectra were taken by using a Varian E-9 X-band spectrometer. A gas-flow cavity insert was used to collect spectra at near (130 K) liquid-nitrogen temperatures.

X-ray powder diffraction patterns were collected for compounds **1** and **4** on a Norelco (Philips Electronics Co.) powder diffractometer or a Scintag PAD II system, both of which used graphite-monochromated Cu Kα radiation.

X-ray Crystallography. Data Collection, Structure Solution, and Refinement.³⁴ Suitable crystals were mounted on a glass fiber (**1**) or in

Table I. Summary of Crystallographic Data and Data Collection Parameters

parameter	Rh ₂ (O ₂ CCF ₃) ₄ -(Tempo) ₂ (1)	Rh ₂ (O ₂ CC ₃ F ₇) ₄ -(Tempo) ₂ (2)
formula	Rh ₂ F ₁₂ O ₁₀ N ₂ C ₂₆ H ₃₆	Rh ₂ F ₂₈ O ₁₀ N ₂ C ₃₄ H ₃₆
space group	P1	P2 ₁ /c
temp, K	295 ± 5	143 ± 10
<i>a</i> , Å	8.715 (2)	11.450 (2)
<i>b</i> , Å	10.765 (3)	16.604 (3)
<i>c</i> , Å	11.501 (3)	13.163 (2)
α, deg	107.18 (2)	90.0
β, deg	103.30 (2)	90.30 (1)
γ, deg	107.61 (2)	90.0
<i>V</i> , Å ³	920 (1)	2502 (1)
<i>d</i> _{calcd} , g/cm ³	1.751	1.819
<i>Z</i>	1	2
FW	970.38	1370.44
cryst size, mm	0.1 × 0.2 × 0.3	0.25 × 0.25 × 0.25
μ, cm ⁻¹	85.236 (Cu Kα)	7.994 (Mo Kα)
radiation	graphite-monochromated Cu Kα (λ _a = 1.54184 Å)	graphite-monochromated Mo Kα (λ _a = 0.71073 Å)
scan type	θ–2θ	θ–2θ
scan rate, deg/min	2.00–19.53	fixed, 4.00
scan width, deg	2.0	2.0
data collection range	+ <i>h</i> , ± <i>k</i> , ± <i>l</i> (3° < 2θ < 120°)	+ <i>h</i> , + <i>k</i> , ± <i>l</i> (3° < 2θ < 55°)
no. of unique data	2669	5094
no. of data, <i>I</i> > <i>nσ</i> (<i>I</i>)	2479 (<i>n</i> = 2.33)	3409 (<i>n</i> = 3)
no. of variables	332	400
<i>R</i> ₁ ^a	0.0355	0.0614
<i>R</i> ₂ ^b	0.0442	0.0669
esd	1.848	
largest peak, e/Å ³ c	0.29	1.08
Δ/σ ^d	0.24	1.24

^a $R_1 = \sum |F_o| - |F_c| / \sum |F_o|$. ^b $R_2 = [\sum w(|F_o| - |F_c|)^2 / \sum w|F_o|^2]^{1/2}$. ^c Largest peak in the final difference Fourier map. ^d Largest shift (Δ)-to-error (σ) ratio in the final least-squares cycle.

capillary tubing (**2**) with epoxy cement and examined on a Syntex P2₁ autodiffractometer. Crystallographic data and data collection parameters appear in Table I for **1** and **2**. Details of data collection techniques and derivation of the intensity and its standard deviation followed previously published procedures.³⁵ Both data sets were corrected for Lorentz and polarization effects.

For Rh₂(O₂CCF₃)₄(Tempo)₂ (**1**) an empirical absorption correction was applied to the data. Maximum, minimum, and average transmission factors for **1** corresponded to 0.992, 0.508, and 0.768, respectively. The structure solution to **1** proceeded straightforwardly from three-dimensional Patterson maps followed by successive least-squares refinement cycles and difference Fourier maps. During the final stages of the refinement, the six fluorine atoms were found to be slightly disordered on the trifluoroacetate groups. The major and minor occupancy factors were found to be 0.90 and 0.10, respectively. Anisotropic thermal parameters were assigned to all 26 non-hydrogen atoms with isotropic thermal parameters given to the six fluorine atoms (denoted *F_n'Am*; *n* = 1, 2, 3; *m* = 1, 2) that occupied minor positions. The positions of the 18 hydrogen atoms associated with the Tempo ligand were obtained from a difference Fourier map, and all positional and isotropic thermal parameters were refined for these atoms. An extinction correction was made according to the equation $|F_o| = |F_c|(1 + gI_2)^{-1}$, where the value of *g* determined from least-squares refinement was found to be 5.87 × 10⁻⁶.

In contrast to the ease with which the refinement of **1** proceeded to relatively low discrepancy factors, the refinement of Rh₂(O₂CC₃F₇)₄(Tempo)₂ with use of a room temperature Mo Kα data set was arrested at the values of the residuals (*R*₁ = 0.112, *R*₂ = 0.159) reported in the preliminary communication.²⁹ Large thermal motion was evident in each of the C₃F₇ chains suggestive of disorder, but no suitable model could be constructed that permitted the refinement to proceed. Finally, a new

(34) Crystallographic computing was performed on PDP 11/34 and VAX 11/780 computers located at Monsanto Co. with the Enraf-Nonius SDP-PLUS (4th ed., B. A. Frenz and Associates, College Station, TX, 1981) and SHELX-76 (Sheldrick, G. M. In *Computing in Crystallography*; Schenk, H., Olthof-Hazekamp, R., Van Koningsveld, H., Bassi, G. C., Eds.; Delft University Press: Delft, The Netherlands, 1978; pp 34–42) software packages with local modifications.

(35) For example: Besecker, C. J.; Day, V. W.; Klempner, W. G.; Thompson, M. R. *J. Am. Chem. Soc.* **1984**, *106*, 4125–4136.

(32) Johnson, S. A.; Hunt, H. R.; Neuman, H. M. *Inorg. Chem.* **1963**, *2*, 960–962.

(33) Cotton, F. A.; Norman, J. G., Jr. *J. Coord. Chem.* **1971**, *1*, 161–172.

crystal was selected that was cut from another large (vide supra) prism. X-ray data were collected with this new crystal embedded in a glass capillary tube in a liquid-nitrogen cooled (143 K) gas stream. The unit cell parameters for **2** reported in Table I reflect a contraction in the unit cell lengths with an overall shrinkage in the unit cell volume from 2578 (295 K) to 2502 Å³ (143 K). No change in the space group was evident upon cooling the crystal.

An empirical absorption correction was also made to the X-ray data for **2** by use of ψ -scans. Maximum, minimum, and average transmission factors for this crystal were 0.998, 0.632, and 0.863, respectively. The structure solution to **2** was accomplished through a combination of Patterson synthesis, full-matrix least-squares refinement, and difference Fourier cycles. Isotropic full-matrix least-squares refinement of the 38 non-hydrogen atoms in the asymmetric unit converged at conventional residuals of $R_1 = 0.149$ and $R_2 = 0.156$ (see Table I, footnotes *a* and *b*, for *R*-value definitions) for 3409 reflections with $I > 3\sigma(I)$ and $2\theta(\text{Mo K}\alpha) < 54.90^\circ$. At this point the structure was again found to possess a high degree of disorder in the atoms of the heptafluoropropyl groups. Assignment of anisotropic thermal parameters to the C and F atoms of the two independent C₃F₇ groups resulted in poor C–C and C–F bond lengths and very large thermal parameters. This model for the refinement converged with $R_1 = 0.108$ and $R_2 = 0.120$. A difference Fourier map calculated by using the phases from the model with isotropic thermal parameters contained numerous peaks corresponding to the disordered carbon and fluorine positions.

After several attempts the following model emerged to account for disorder in the C₃F₇ groups. For the heptafluoropropyl group with atoms labeled C2A1 through C4A1 and F1A1 through F7A1, a second terminal carbon position was found (C4'A1) containing only one unique fluorine atom, F7'A1. The positions of the other two fluorine atoms were in the direction of the atoms labeled C4A1 and F5A1 through F7A1. Much more severe disorder occurred in the second C₃F₇ group. Carbon atoms C2A2, C3A2, and C4A2 appeared to have rather well-defined positions. The fluorine atoms bonded to C2A2 were represented by three positions denoted by F1A2, F2A2, and F2'A2. For C3A2 four fluorine atom positions were found: F3A2, F3'A2, F4A2, and F4'A2. The terminal C4A2 carbon was found to have some six fluorine atoms within bonding distances: F5A2, F5'A2, F6A2, F6'A2, F7A2, and F7'A2. Independent refinement of the disordered positions of the heptafluoropropyl groups was not possible.

To complete the structure solution a constrained refinement was employed from the SHELX-76 program package. For the atoms of the heptafluoropropyl groups, C–C and C–F distance constraints were set and refined by using the DFIX option with corresponding distance and σ values of 1.540 and 0.040 for C–C interactions and 1.350 and 0.040 for C–F interactions. Initial cycles of the constrained refinement assumed statistical disordering between the C and F positions. Atoms of the heptafluoropropyl groups were refined with isotropic thermal parameters at this point. With anisotropic temperature factors for the remaining atoms in **2**, the structure converged to residuals of $R_1 = 0.089$ and $R_2 = 0.097$ for the 3409 observed reflections. Now refinement of the site occupancy factors for the C and F atoms of the C₃F₇ groups gave an indication of the relative degree of disorder for each atom position. The final cycles of constrained block-diagonal least-squares refinement employed a $1/\sigma^2$ weighting scheme and included anisotropic temperature factors for 45 of the 46 ordered and disordered non-hydrogen atoms, fixed site occupancy factors for 19 of the 28 ordered and disordered atoms of the C₃F₇ groups as listed in Table III, and hydrogen atoms contributions with the positions of these atoms calculated with an idealized geometry and a C–H distance of 1.08 Å. The final residuals at convergence are listed in Table I. A final difference Fourier map revealed that the highest peak was located by C4'A1.

Tables of observed and calculated structure factors for those reflections used in the refinements for **1** and **2** are available as supplementary material.³⁶

Results

Tables II and III record the final atomic positional and isotropic equivalent thermal parameters for **1** and **2**, respectively. The anisotropic thermal parameters for **1** and **2** are listed in Tables IIS and IIIS.³⁶ Bond distances and angles for **1** and **2** appear in Tables IV and V, respectively, and these tables include some key nonbonded contacts as well. Bond distances and angles involving the refined hydrogen atoms in **1** are given in Table IVS,³⁶ while the bond distances and angles involving the heptafluoropropyl substituents in **2** are tabulated in Table VS.³⁶ Least-squares plane

Table II. Atomic Fractional Coordinates ($\times 10^4$ except $\times 10^3$ for Fn' and H) and Thermal Parameters (\AA^2 , B_{iso} for Fn' and H) for $\text{Rh}_2(\text{O}_2\text{CCF}_3)_4(\text{Tempo})_2$ (**1**)^a

atom	<i>x</i>	<i>y</i>	<i>z</i>	B_{eq}^b
Rh	70.1 (3)	953.0 (3)	-364.8 (2)	2.825 (6)
N1TR	-107 (4)	3073 (3)	-1890 (3)	3.6 (1)
C2TR	1139 (7)	3269 (5)	-2610 (5)	5.6 (1)
C3TR	995 (8)	4400 (6)	-3128 (5)	7.5 (2)
C4TR	-748 (9)	4254 (6)	-3762 (5)	7.4 (2)
C5TR	-1735 (7)	4250 (5)	-2850 (5)	5.8 (1)
C6TR	-1857 (6)	3076 (5)	-2340 (4)	4.6 (1)
O7T	325 (4)	2823 (3)	-873 (3)	4.4 (1)
C8T	2924 (7)	3753 (7)	-1644 (7)	7.7 (2)
C9T	636 (9)	1806 (7)	-3695 (6)	8.5 (2)
C10T	-2443 (7)	3389 (7)	-1165 (6)	6.5 (2)
C11T	-3126 (8)	1647 (6)	-3381 (6)	6.6 (2)
O1A1	1882 (4)	510 (3)	2028 (3)	3.9 (1)
O2A1	2026 (4)	2284 (3)	1344 (3)	3.9 (1)
C1A1	2439 (5)	1768 (4)	2139 (4)	3.4 (1)
C2A1	3771 (6)	2832 (5)	3461 (4)	4.6 (1)
F1A1	4668 (5)	2275 (4)	4024 (4)	9.3 (1)
F2A1	3025 (5)	3351 (5)	4204 (3)	9.1 (1)
F3A1	4868 (5)	3910 (4)	3374 (4)	8.6 (1)
O1A2	-1603 (4)	1315 (5)	529 (3)	4.0 (1)
O2A2	-1734 (4)	-474 (3)	1203 (3)	3.9 (1)
C1A2	-2083 (5)	546 (4)	1115 (4)	3.6 (1)
C2A2	-3202 (6)	949 (5)	1879 (4)	4.7 (1)
F1A2	-4219 (4)	1447 (4)	1305 (4)	8.3 (1)
F2A2	-4153 (5)	-74 (4)	2050 (4)	12.0 (1)
F3A2	-2232 (5)	2002 (5)	2975 (4)	10.2 (1)
F1'A1 ^c	338 (3)	238 (3)	442 (3)	5.6 (6)
F2'A1 ^c	523 (4)	304 (3)	365 (3)	6.7 (7)
F3'A1 ^c	388 (4)	397 (3)	373 (3)	6.3 (7)
F1'A2 ^c	-282 (3)	71 (2)	296 (2)	3.5 (4)
F2'A2 ^c	-319 (3)	213 (3)	209 (2)	4.8 (5)
F3'A2 ^c	-466 (3)	29 (3)	135 (2)	4.6 (5)
H1C3T	180 (6)	547 (6)	-222 (5)	7 (2)
H2C3T	161 (6)	456 (5)	-342 (5)	7 (2)
H1C4T	-64 (7)	512 (6)	-387 (5)	8 (2)
H2C4T	-118 (5)	344 (5)	-439 (4)	5 (1)
H1C5T	-116 (5)	517 (4)	-205 (4)	4 (1)
H2C5T	-316 (6)	400 (5)	-325 (5)	6 (1)
H1C8T	331 (6)	307 (5)	-119 (5)	7 (1)
H2C8T	370 (8)	403 (7)	-200 (6)	12 (2)
H3C8T	312 (7)	470 (6)	-76 (5)	8 (2)
H1C9T	-73 (8)	141 (6)	-461 (6)	10 (2)
H2C9T	115 (9)	100 (7)	-316 (7)	14 (3)
H3C9T	158 (7)	191 (6)	-406 (5)	8 (2)
H1C10T	-145 (7)	440 (6)	-38 (5)	8 (2)
H2C10T	-247 (8)	267 (6)	-82 (6)	10 (2)
H3C10T	-362 (7)	343 (6)	-142 (6)	9 (2)
H1C11T	-480 (10)	165 (96)	-369 (8)	17 (3)
H2C11T	-310 (7)	90 (5)	-310 (5)	8 (2)
H3C11T	-273 (6)	149 (5)	-407 (5)	6 (1)

^aNumbers in parentheses are the estimated standard deviations in the least significant figure. ^bThe form of the equivalent isotropic thermal parameter is the following: $(4/3)[a^2B(1,1) + b^2B(2,2) + c^2B(3,3) + ab(\cos \gamma)B(1,2) + ac(\cos \beta)B(1,3) + bc(\cos \alpha)B(2,3)]$. ^cPrimed atoms represent disordered positions with a site occupancy factor of 0.10. The corresponding unprimed atoms have site occupancy factors of 0.90.

calculations for **1** and **2** appear in Tables VIS1 and VIS2, respectively. Both structures **1** and **2** confirm that the Tempo ligands coordinate through the oxygen atoms to the axial positions of the $\text{Rh}_2(\text{O}_2\text{CR})_4$ frameworks with two nitroxyl ligands per dinuclear cluster. A detailed description of the molecular structures of **1** and **2** will now be presented.

Rh₂(O₂CCF₃)₄(Tempo)₂ (1**).** This molecule crystallizes in a triclinic unit cell containing one formula unit with a crystallographic center of inversion located at the midpoint of the Rh–Rh bond. Figure 1 displays the coordinated biradical **1** with the atom labeling scheme shown. The $\text{Rh}_2(\text{O}_2\text{C})_4$ core approximates D_{4h} symmetry, and the bond distances and angles involving the Rh atoms and the trifluoroacetate ligands agree well with previous structures of this type.^{23,24} As with other structures containing

(36) See the paragraph at the end of this paper regarding supplementary material.

Table III. Atomic Fractional Coordinates ($\times 10^4$) and Thermal Parameters (\AA^2) for $\text{Rh}_2(\text{O}_2\text{CC}_3\text{F}_7)_4(\text{Tempo})_2$ (2)^a

atom	x	y	z	B_{eq}^b
Rh	-414.6 (4)	660.2 (3)	171.6 (4)	3.16 (2)
N1TR	-1767 (5)	2390 (3)	103 (4)	3.5 (2)
C2TR	-1060 (6)	2973 (4)	-508 (6)	4.1 (2)
C3TR	-1760 (8)	3767 (4)	-649 (6)	5.5 (2)
C4TR	-3039 (8)	3649 (5)	-907 (6)	5.9 (3)
C5TR	-3600 (6)	3165 (5)	-48 (6)	5.0 (2)
C6TR	-3079 (6)	2333 (5)	95 (5)	4.0 (2)
O7T	-1206 (4)	1842 (3)	597 (3)	3.8 (1)
C8TR	-810 (6)	2585 (4)	-1555 (5)	4.7 (2)
C9T	67 (8)	3131 (5)	55 (6)	5.8 (3)
C10T	-3450 (6)	1982 (6)	1145 (6)	6.2 (3)
C11T	-3433 (6)	1735 (6)	-729 (6)	5.6 (3)
O1A1	396 (4)	633 (3)	1555 (4)	4.1 (1)
O2A1	1172 (4)	-597 (3)	1221 (4)	4.0 (1)
O1A2	1052 (4)	1131 (3)	-464 (4)	3.9 (1)
O2A2	1828 (4)	-93 (3)	-782 (4)	4.0 (1)
C1A1	996 (6)	27 (5)	1733 (6)	4.2 (2)
C2A1	1638 (6)	33 (5)	2770 (6)	5.6 (3)
C3A1	2647 (16)	617 (8)	2911 (15)	14.4 (6)
C4A1	3617 (15)	661 (12)	2392 (21)	25.6 (18)b
C4'A1 ^c	3698 (40)	1035 (20)	3517 (42)	15.8 (5)d*
C1A2	1791 (5)	668 (4)	-792 (5)	3.7 (2)
C2A2	2851 (6)	1062 (5)	-1327 (6)	5.0 (2)
C3A2	2546 (10)	1233 (6)	-2487 (10)	9.5 (5)
C4A2	3435 (10)	1559 (8)	-3195 (8)	10.0 (5)
F1A1	2041 (6)	-696 (3)	2999 (4)	8.0 (2)
F2A1	891 (6)	228 (4)	3508 (4)	9.1 (3)
F3A1	2097 (8)	1383 (5)	2929 (8)	13.8 (4)
F4A1	3092 (10)	515 (8)	4010 (6)	11.9 (5)b
F5A1	3129 (8)	806 (8)	1509 (6)	12.6 (5)b
F6A1	4431 (9)	1171 (8)	2724 (10)	13.7 (6)b
F7A1	3904 (11)	-84 (9)	2211 (13)	16.5 (7)b
F7'A1 ^c	4130 (24)	226 (13)	3609 (36)	13.9 (5)d
F1A2	3753 (5)	581 (5)	-1327 (9)	15.2 (4)
F2A2	3107 (6)	1756 (4)	-913 (6)	9.2 (2)b
F2'A2 ^c	3652 (48)	811 (40)	-640 (34)	22.8 (10)d
F3A2	1549 (17)	1252 (30)	-2662 (16)	37.1 (12)b
F3'A2 ^c	1715 (20)	750 (12)	-2892 (19)	4.4 (5)d
F4A2	2586 (33)	424 (15)	-2769 (13)	35.8 (17)b
F4'A2 ^c	1807 (13)	1967 (9)	-2373 (17)	3.6 (4)d
F5A2	4126 (19)	2082 (13)	-2776 (16)	10.5 (8)c
F5'A2 ^c	4335 (19)	1546 (19)	-2638 (21)	13.6 (13)c
F6A2	4025 (13)	886 (8)	-3532 (13)	8.5 (5)c
F6'A2 ^c	2385 (33)	2085 (16)	-2954 (39)	35.4 (22)c
F7A2	3067 (13)	1867 (12)	-4045 (12)	9.5 (7)c
F7'A2 ^c	2825 (37)	1141 (26)	-3981 (15)	24.7 (25)c

^aNumbers in parentheses are the estimated standard deviations in the least significant figure. ^bThe form of the isotropic equivalent thermal parameter is the following: $(4/3)[a^2B(1,1) + b^2B(2,2) + c^2B(3,3) + ab(\cos \gamma)B(1,2) + ac(\cos \beta)B(1,3) + bc(\cos \alpha)B(2,3)]$. Letters following thermal parameters are site occupancy codes. The asterisk denotes an atom refined with a B_{50} value. ^cPrimed atoms represent disordered positions. Site occupancy factor codes: b, 0.75; c, 0.50; d, 0.25.

trifluoroacetate ligands (e.g., see ref 33), some rotational disorder was found in the fluorine atoms of the two unique CF_3 groups. Major (90%) and minor (10%) orientations of the fluorine atoms were observed and refined. In the trans positions to the Rh–Rh bond of 2.417 (1) \AA in length are nitroxyl oxygen atoms at 2.220 (2) \AA from each Rh center. The axial nitroxyl oxygen atoms are nearly colinear with the Rh–Rh bond ($\angle \text{Rh}'\text{-Rh-O} = 175.44$ (6) $^\circ$) and at a distance from each Rh atom that is in accord with other oxygen-bonded adducts of $\text{Rh}_2(\text{O}_2\text{CCF}_3)_4$.²⁷ Each Rh atom is displaced 0.080 \AA out of the equatorial plane of four trifluoroacetate oxygen atoms toward the axial nitroxyl oxygen atom.

The coordinated Tempo ligands in **1** produce an Rh–O7T–N1TR angle of 138.0 (1) $^\circ$, and the C_2NO group makes an acute dihedral angle with the equatorial plane of trifluoroacetate oxygen atoms of 52.0 $^\circ$. The conformation of the nitroxyl C_2NO group, which will be discussed in more detail in the next section, is defined by the angle α that corresponds to the out-of-plane acute angle between the N–O bond and the C_2N plane. In **1** the value of α is only 3.0 $^\circ$. The nitroxyl oxygen atom rises only 0.067 \AA out

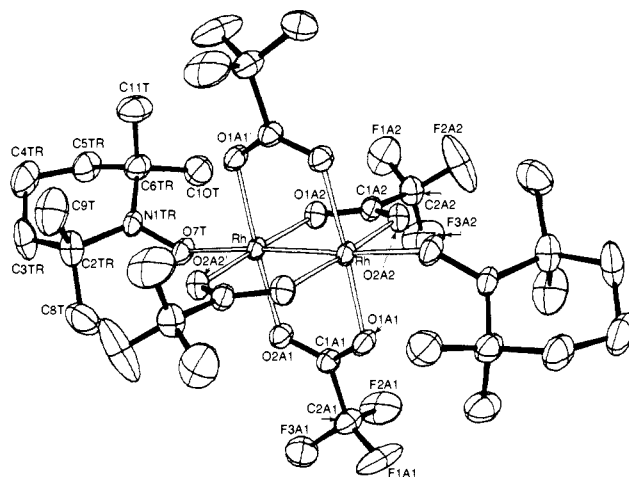


Figure 1. Molecular structure of $\text{Rh}_2(\text{O}_2\text{CCF}_3)_4(\text{Tempo})_2$ (**1**) showing the atom labeling scheme. Thermal ellipsoids are drawn at the 50% probability level. The molecule resides on a crystallographic center of inversion located at the midpoint of the Rh–Rh bond.

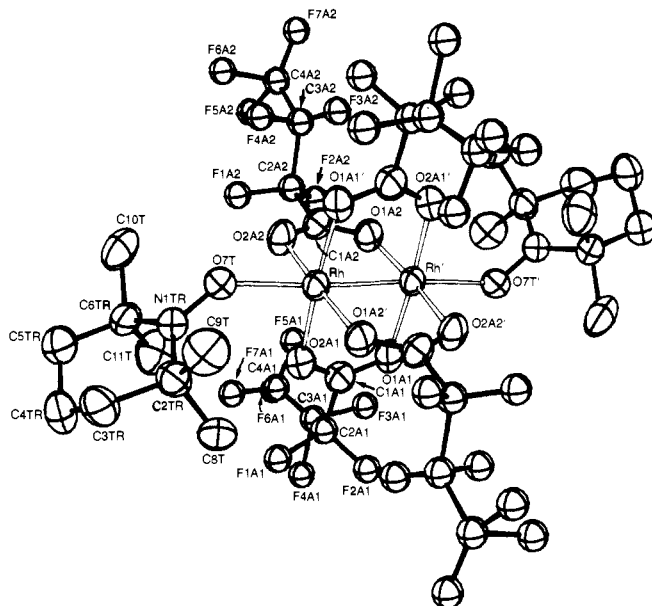


Figure 2. ORTEP drawing of $\text{Rh}_2(\text{O}_2\text{CC}_3\text{F}_7)_4(\text{Tempo})_2$ (**2**) showing the atom labeling scheme. For the disordered C_3F_7 groups, only the major orientation is shown. The carbon and fluorine atoms of the heptafluoropropyl groups are assigned arbitrarily small isotropic thermal ellipsoids while the remaining atoms show anisotropic thermal ellipsoids at the 50% probability level. Primed and unlabeled atoms are related to unprimed atoms by a center of inversion located at the midpoint of the Rh–Rh bond.

of the C_2N plane. The piperidine ring of the Tempo ligand adopts a somewhat flattened chair conformation. Bond distances and angles about the piperidine ring appear normal.

The structure of **1** contains hydrogen atoms that are attached only to aliphatic carbon atoms. All oxygen atoms in **1** are coordinated to the Rh atoms, and no hydrogen bonding occurs in the molecular packing interactions in the lattice. While molecules of $\text{Rh}_2(\text{O}_2\text{CCF}_3)_4(\text{Tempo})_2$ occur as discrete units in the lattice, intermolecular through-space contacts between nitroxyl groups are a key consideration in light of the strong antiferromagnetic exchange interaction (vide infra). These contacts will be examined in detail in the Discussion section.

$\text{Rh}_2(\text{O}_2\text{CC}_3\text{F}_7)_4(\text{Tempo})_2$ (2**).** Two formula units of **2** crystallize in a monoclinic unit cell with each dirhodium(II) complex residing on a crystallographic center of inversion at the midpoint of the Rh–Rh bond. Figure 2 depicts the dinuclear unit in **2** with the atom labeling scheme given for the major positions of the disordered C_3F_7 substituents. Figure 1S³⁶ defines the disorder model

Table IV. Bond Distances (Å) and Angles (deg) for Rh₂(O₂CCF₃)₄(Tempo)₂ (1)^a

Distances			
Rh-Rh'	2.417 (1)	O2A1-C1A1	1.243 (4)
Rh-O1A1'	2.034 (2)	O1A2-C1A2	1.250 (4)
Rh-O2A1	2.034 (2)	O2A2-C1A2	1.251 (4)
Rh-O1A2	2.033 (2)	O7T...O7T'	6.853 (3)
Rh-O2A2'	2.025 (2)	O7T...O7T*	4.784 (3)
Rh-O7T	2.220 (2)	O7T-N1TR	1.275 (3)
Rh...O7T'	4.634 (2)	O7T...N1TR	7.867 (3)
Rh...N1TR	3.287 (2)	O7T...N1TR*	4.706 (3)
Rh...N1TR'	5.674 (2)	N1TR...N1TR'	8.948 (3)
F1A1-C2A1	1.293 (5)	N1TR...N1TR*	4.966 (3)
F1'A1-C2A1	1.401 (27) ^b	N1TR-C2TR	1.512 (5)
F2A1-C2A1	1.288 (5)	N1TR-C6TR	1.496 (5)
F2'A1-C2A1	1.171 (31)	C1A1-C2A1	1.524 (5)
F3A1-C2A1	1.309 (5)	C1A2-C2A2	1.528 (5)
F3'A1-C2A1	1.142 (3)	C2TR-C3TR	1.529 (7)
F1A2-C2A2	1.316 (5)	C2TR-C8T	1.516 (7)
F1'A2-C2A2	1.336 (20)	C2TR-C9T	1.547 (7)
F2A2-C2A2	1.261 (5)	C3TR-C4TR	1.464 (9)
F2'A2-C2A2	1.218 (24)	C4TR-C5TR	1.502 (8)
F3A2-C2A2	1.294 (5)	C5TR-C6TR	1.530 (6)
F3'A2-C2A2	1.154 (23)	C6TR-C10T	1.534 (7)
O1A1-C1A1	1.248 (4)	C6TR-C11T	1.515 (6)

Angles			
Rh'-Rh-O1A1'	87.36 (6)	O2A1-Rh-O7T	87.61 (9)
Rh'-Rh-O2A1	87.96 (6)	O1A2-Rh-O2A2	175.61 (9)
Rh'-Rh-O1A2	87.83 (7)	O1A2-Rh-O7T	90.9 (1)
Rh'-Rh-O2A2	87.79 (7)	O2A2-Rh-O7T	93.5 (1)
Rh'-Rh-O7T	175.44 (6)	Rh-O1A1'-C1A1	117.9 (1)
F1A1-C2A1-F2A1	109.4 (4)	Rh-O2A1-C1A1	117.3 (1)
F1A1-C2A1-F3A1	106.4 (4)	Rh-O1A2-C1A2	117.2 (1)
F1A1-C2A1-C1A1	112.3 (3)	Rh-O2A2'-C1A2'	117.6 (1)
F2A1-C2A1-F3A1	106.2 (4)	Rh-O7T-N1TR	138.0 (1)
F2A1-C2A1-C1A1	110.1 (3)	O7T-N1TR...O7T*	85.7 (3)
F3A1-C2A1-C1A1	112.2 (3)	O7T-N1TR...N1TR*	94.3 (3)
F1'A1-C2A1-F2'A1	105.1 (21)	O7T-N1TR-C2TR	118.3 (3)
F1'A1-C2A1-F3'A1	108.7 (22)	O7T-N1TR-C6TR	117.8 (3)
F1'A1-C2A1-C1A1	108.7 (1)	C2TR-N1TR-C6TR	123.9 (3)
F2'A1-C2A1-F3'A1	98.9 (23)	O1A1-C1A1-O2A1	129.4 (3)
F2'A1-C2A1-C1A1	119.1 (15)	O1A1-C1A1-C2A1	115.2 (3)
F3'A1-C2A1-C1A1	115.5 (16)	O2A1-C1A1-C2A2	115.4 (3)
F3'A1-C2A1-F2A2	106.7 (5)	O1A2-C1A2-O2A2	129.5 (3)
F3'A1-C2A1-F3A2	103.6 (4)	O1A2-C1A2-C2A2	115.3 (3)
F3'A1-C2A1-C1A2	112.5 (3)	O2A2-C1A2-C2A2	115.2 (3)
F2A2-C2A2-F3A2	111.0 (5)	N1TR-C2TR-C3TR	107.2 (4)
F2A2-C2A2-C1A2	113.2 (4)	N1TR-C2TR-C8T	107.4 (4)
F3A2-C2A2-C1A2	109.4 (4)	N1TR-C2TR-C9T	107.2 (4)
F1'A2-C2A2-F2'A2	112.1 (16)	C3TR-C2TR-C8T	111.2 (5)
F1'A2-C2A2-F3'A2	105.5 (16)	C3TR-C2TR-C9T	113.3 (5)
F1'A2-C2A2-C1A2	108.7 (9)	C8T-C2TR-C9T	110.3 (5)
F2'A2-C2A2-F3'A2	99.2 (18)	C2TR-C3TR-C4TR	116.3 (5)
F2'A2-C2A2-C1A2	116.2 (12)	C3TR-C4TR-C4TR	110.5 (5)
F3'A2-C2A2-C1A2	114.4 (12)	C4TR-C5TR-C6TR	113.5 (4)
O1A1'-Rh-O2A1	175.33 (8)	N1TR-C6TR-C5TR	108.5 (3)
O1A1'-Rh-O1A2'	91.9 (1)	N1TR-C6TR-C10T	107.8 (3)
O1A1'-Rh-O2A2	88.1 (1)	N1TR-C6TR-C11T	110.7 (4)
O1A1'-Rh-O7T	97.05 (9)	C5TR-C6TR-C10T	109.6 (4)
O2A1-Rh-O1A2	88.3 (1)	C5TR-C6TR-C11T	110.9 (4)
O2A1-Rh-O2A2	91.3 (1)	C10T-C6TR-C11T	109.2 (4)

^a Primed atoms are related to unprimed ones by an intramolecular center of inversion. Some important nonbonded contacts (···) are included in this table. Intermolecular contacted atoms are succeeded by a superscripted asterisk. Distances and angles involving the hydrogen atoms appear in Table IVS. ^b Fluorine atoms comprising the minor orientation of the CF₃ groups are marked with a prime at the center of the label.

for the C₃F₇ groups. Aside from the presence of the C₃F₇ substituents in **2**, the *molecular* structure of **2** is closely similar to **1**. The Rh-Rh bond length in **2** is 2.431 (1) Å, a value significantly longer than that in **1**. In addition to the direct Rh-Rh bond, each Rh atom in **2** is coordinated by four heptafluorobutyrate oxygen atoms in an equatorial plane with an average Rh-O bond length of 2.036 (5) Å. Trans to the Rh-Rh bond is a Tempo oxygen atom at 2.235 (5) Å from each Rh atom and colinear to the Rh-Rh bond with an Rh'-Rh-O7T angle of 176.0 (1)°. Each

Table V. Bond Distances (Å) and Angles (deg) for Rh₂(O₂CC₃F₇)₄(Tempo)₂ (**2**)^a Excluding the Heptafluoropropyl Substituents

Distances			
Rh-Rh'	2.431 (1)	O7T'...N1TR	7.864 (7)
Rh-O1A1'	2.039 (5)	O7T...N1TR*	6.104 (7)
Rh-O2A1	2.027 (5)	O7T*...N1TR	7.361 (7)
Rh-O1A2'	2.035 (4)	N1TR...N1TR'	8.913 (7)
Rh-O2A2	2.042 (4)	N1TR...N1TR*	6.591 (7)
Rh-O7T	2.235 (5)	N1TR-C2TR	1.499 (9)
Rh...O7T'	4.663 (5)	N1TR-C6TR	1.505 (9)
Rh...N1TR	3.266 (5)	C1A1-C2A1	1.547 (12)
Rh...N1TR'	5.659 (5)	C1A2-C2A2	1.551 (10)
O1A1-C1A1	1.240 (9)	C2TR-C3TR	1.554 (11)
O2A1-C1A1	1.252 (9)	C2TR-C8T	1.549 (10)
O1A2-C1A2	1.224 (8)	C2TR-C9T	1.508 (11)
O2A2-C1A2	1.264 (9)	C3TR-C4TR	1.515 (13)
O7T...O7T'	6.896 (7)	C4TR-C5TR	1.532 (12)
O7T...O7T*	6.935 (7)	C5TR-C6TR	1.516 (11)
O7T-N1TR	1.288 (7)	C6TR-C10T	1.561 (11)
		C6TR-C11T	1.523 (12)

Angles			
Rh'-Rh-O1A1'	88.3 (1)	O7T-N1TR-C6TR	117.0 (5)
Rh'-Rh-O2A1	87.2 (1)	C2TR-N1TR-C6TR	125.4 (5)
Rh'-Rh-O1A2'	86.9 (1)	O1A1-C1A1-O2A1	131.3 (7)
Rh'-Rh-O2A2	88.2 (1)	O1A1-C1A1-C2A1	114.9 (7)
Rh'-Rh-O7T	176.0 (1)	O2A1-C1A1-C2A1	113.8 (6)
O1A1'-Rh-O2A1	175.5 (2)	O1A1-C1A2-O2A2	130.4 (6)
O1A1'-Rh-O1A2'	90.2 (2)	O1A2-C1A2-C2A2	116.1 (6)
O1A1'-Rh-O2A2	89.8 (2)	O2A2-C1A2-C2A2	113.6 (6)
O1A1'-Rh-O7T	88.8 (2)	N1TR-C2TR-C3TR	109.4 (6)
O2A1-Rh-O1A2'	89.9 (2)	N1TR-C2TR-C8T	108.2 (6)
O2A1-Rh-O2A2	89.7 (1)	N1TR-C2TR-C9T	108.2 (6)
O2A1-Rh-O7T	95.7 (1)	C3TR-C2TR-C8T	110.1 (6)
O1A2'-Rh-O2A2	175.7 (1)	C3TR-C2TR-C9T	110.5 (7)
O1A2'-Rh-O7T	95.9 (2)	C8T-C2TR-C9T	110.4 (6)
O2A2-Rh-O7T	89.0 (1)	C2TR-C3TR-C4TR	114.5 (7)
Rh-O1A1'-C1A1'	115.8 (5)	C3TR-C4TR-C5TR	108.1 (7)
Rh-O2A1-C1A1	117.4 (4)	C4TR-C5TR-C6TR	113.8 (7)
Rh-O1A2'-C1A2'	118.5 (4)	N1TR-C6TR-C5TR	109.6 (6)
Rh-O2A2-C1A2	116.0 (3)	N1TR-C6TR-C10T	107.1 (6)
Rh-O7T-N1TR	134.2 (4)	N1TR-C6TR-C11T	107.9 (6)
O7T-N1TR...O7T*	65.6 (4)	C5TR-C6TR-C10T	109.6 (6)
O7T-N1TR...N1TR*	62.5 (4)	C5TR-C6TR-C11T	113.7 (6)
O7T-N1TR-C2TR	117.3 (5)	C10T-C6TR-C11T	108.3 (7)

^a Primed atoms are related to unprimed ones by a crystallographic center of inversion. Some nonbonded contacts (···) are included in this table.

Rh atom is displaced 0.084 Å out of the heptafluorobutyrate oxygen plane toward the axial nitroxyl oxygen atom.

The Tempo oxygen atom in **2** makes a slightly less obtuse Rh-O7T-N1TR angle than in **1** with a value of 134.2 (4)°. The dihedral angle in **2** between the equatorial plane of heptafluorobutyrate oxygen atoms and the C₂NO group is 45.9°, slightly more acute than in **1**. The Tempo ligand in **2** has a somewhat more pyramidal conformation than in **1** with an α angle of 6.5°. The N-O bond has a length of 1.288 (7) Å, and the oxygen atom rises 0.145 Å out of the C₂N plane. Distances and angles about the piperidine ring have typical values with a flattened chair conformation adopted by the six-membered ring.

The structure of **2** consists of discrete dinuclear Rh₂(O₂CC₃F₇)₄(Tempo)₂ units with no significant nonbonded contacts between pairs of such units. As noted above for **1**, a complete analysis of the packing geometries in **1** and **2** will be presented in the Discussion section as these packing interactions relate to the observed magnetic behavior.

Magnetic Susceptibility Data. Variable-temperature (4.2–350 K) magnetic susceptibility data were collected for powdered samples of **1–5**. These data in conjunction with the least-squares fit calculated values to the appropriate equations (vide infra) are compiled in Tables VIISn ($n = 1, \dots, 4$).³⁶

For the Rh₂(O₂CR)₄(Tempo)₂ biradicals **1–3**, a strong anti-ferromagnetic exchange interaction was observed for each compound. In the case of **1**, the effective magnetic moment per nitroxyl (R₂NO) group falls from 1.06 μ_B at 342 K, to 0.80 μ_B

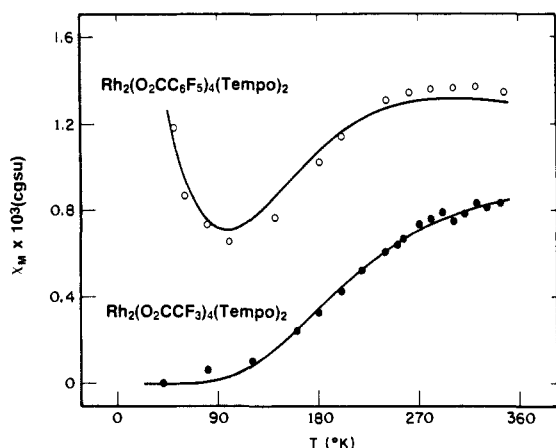


Figure 3. Plots of the experimental molar paramagnetic susceptibilities for $\text{Rh}_2(\text{O}_2\text{CC}_6\text{F}_5)_4(\text{Tempo})_2$ (3, ○) and $\text{Rh}_2(\text{O}_2\text{CCF}_3)_4(\text{Tempo})_2$ (1, ●) vs. temperature. The solid lines represent the least-squares to the Bleaney–Bowers equation with (3, eq 2) and without (1, eq 1) inclusion of a paramagnetic impurity.

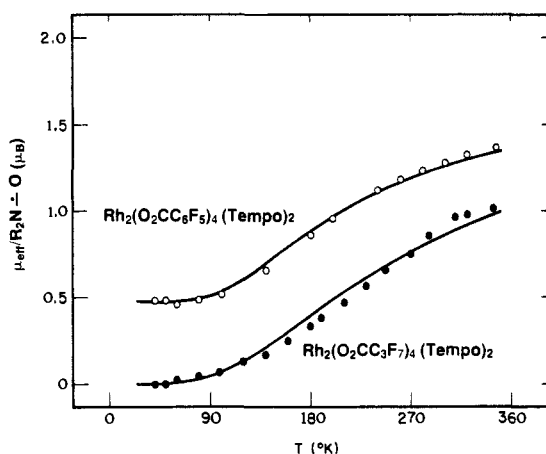


Figure 4. Plots of the derived effective magnetic moments per nitroxyl group vs. temperature for $\text{Rh}_2(\text{O}_2\text{CC}_6\text{F}_5)_4(\text{Tempo})_2$ (3, ○) and $\text{Rh}_2(\text{O}_2\text{CC}_3\text{F}_7)_4(\text{Tempo})_2$ (2, ●). The solid lines were generated from the least-squares fit to the experimental molar paramagnetic susceptibilities (and hence, the μ_{eff} values) according to eq 2 (3) and 1 (2).

at 250 K, and finally to 0.14 μ_B at 80 K. Below 80 K this compound is essentially diamagnetic. The magnetic susceptibility data for 1 are plotted in Figure 3. The corrected molar paramagnetic susceptibility (χ_M) data for 1 were least-squares fit to the form of the Bleaney–Bowers equation³⁷ shown in eq 1, as-

$$\chi_M = \frac{Ng^2\beta^2}{kT} \left[\frac{2}{3 + \exp(-2J/kT)} \right] + N\alpha \quad (1)$$

suming an isotropic exchange Hamiltonian of the form $\hat{H} = -2J\hat{S}_1\hat{S}_2$. In eq 1, $N\alpha$ represents the temperature-independent paramagnetism which in addition to the diamagnetism was corrected for by using a procedure described in the Experimental Section. The resulting least-squares fit parameters for 1 are $J = -239 \text{ cm}^{-1}$ and $g = 2.00$. The solid curve in Figure 3 for 1 represents this best least-squares fit. Similarly, the χ_M data for 2 were least-squares fit to eq 1 for an $S_1 = S_2 = 1/2$ pairwise interaction to produce parameters of $J = -269 \text{ cm}^{-1}$ and $g = 2.00$. Figure 4 presents the experimental effective magnetic moments as a function of temperature and the resulting best least-squares fit curve generated from these data for 2.

For $\text{Rh}_2(\text{O}_2\text{CC}_6\text{F}_5)_4(\text{Tempo})_2$ (3) the magnetic susceptibility data were also indicative of a strong antiferromagnetic exchange interaction. Below 80 K the data suggested the presence of a small

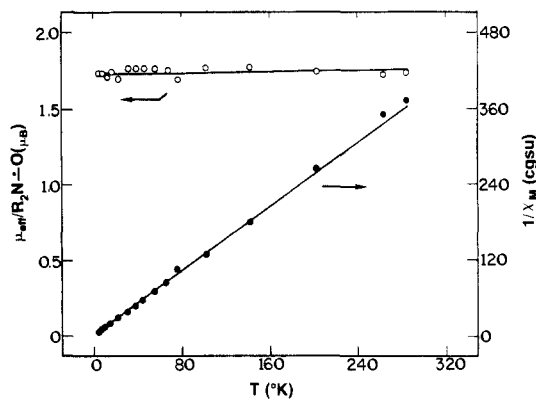


Figure 5. Reciprocal experimental molar paramagnetic susceptibility (●) per binuclear complex and effective magnetic moment (○) per nitroxyl group vs. temperature for $\text{Mo}_2(\text{O}_2\text{CCF}_3)_4(\text{Tempo})_2$ (4). The solid lines represent the least-squares fit to the Curie–Weiss law.

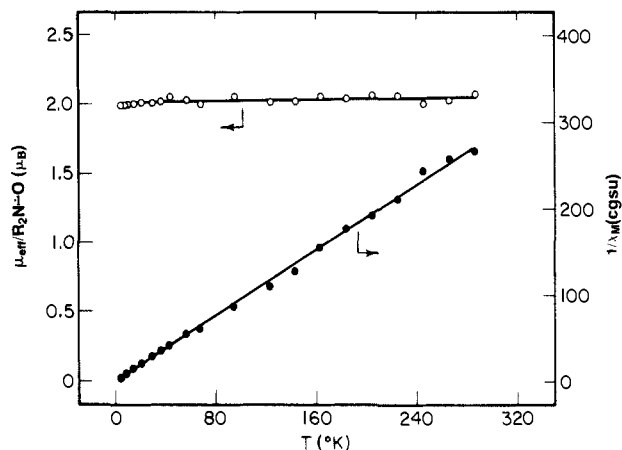


Figure 6. Reciprocal experimental molar paramagnetic susceptibility (●) per binuclear complex and effective magnetic moment (○) per nitroxyl group vs. temperature for $\text{Rh}_2(\text{O}_2\text{CCF}_3)_4(\text{Tempo})_2$ (5). The solid lines represent the least-squares fit to the Curie–Weiss law using the g value determined from the powder EPR spectrum.

amount of paramagnetic ($S = 1/2$) impurity as evidenced by the rising χ_M values at low temperatures. For 3 the χ_M data were fit to an equation of the form shown below, where p gauges the amount of paramagnetic impurity present in the sample (% impurity = $100p$). The least-squares fit χ_M data for 3 produced

$$\chi_M = (1-p) \left(\frac{Ng^2\beta^2}{kT} \right) \left[\frac{2}{3 + \exp(-2J/kT)} \right] + N\alpha + p \left(\frac{Ng^2\beta^2}{4kT} \right) \quad (2)$$

$J = -184 \text{ cm}^{-1}$, $g = 2.00$, and $p = 0.0134$ (e.g., 1.34% $S = 1/2$ impurity). These data are displayed in Figures 3 (χ_M) and 4 (μ_{eff}) and are compared to the corresponding data for 1 and 2. Figure 2S³⁶ compares the μ_{eff} values for 3 with those of 1.

In striking contrast to the strong antiferromagnetic exchange interactions found for 1–3, a sample of $\text{Mo}_2(\text{O}_2\text{CCF}_3)_4(\text{Tempo})_2$ (4) showed no signs of exchange coupling in the magnetic susceptibility data. Figure 5 displays a plot of the μ_{eff} values per nitroxyl group and the reciprocal χ_M data as a function of temperature. Least-squares fitting of the experimental χ_M values to the Curie–Weiss law produced the solid straight lines shown in Figure 5 for the equation $\chi_M^{-1} = 1.2784T + 0.2455$ with a g value of 2.00. From this equation a Curie constant of 0.782 (emu·K)/mol can be calculated with $\theta = -0.192 \text{ K}$.

Magnetic susceptibility data were also collected for $\text{Rh}_2(\text{O}_2\text{CCF}_3)_4(\text{Tempo})_2$ (5) whose structure was previously reported²⁷ to contain only hydrogen-bonded nitroxyl groups. Figure 6 shows the experimental points for effective magnetic moment per nitroxyl group and the reciprocal χ_M data plotted as a function of tem-

(37) Bleaney, B.; Bowers, K. D. *Proc. R. Soc. London, Ser. A* 1952, 214, 451–465.

Table VIII. Solid-State Electronic Spectral Data^a

compound	$\pi^*(\text{Rh}_2) \rightarrow \sigma^*(\text{Rh-O})$	$\pi(\text{Rh-O}) \rightarrow \sigma^*(\text{Rh-O})$	$\delta(\text{Mo}_2) \rightarrow \delta^*(\text{Mo}_2)$	$n \rightarrow \pi^*$	not assigned
$\text{Rh}_2(\text{O}_2\text{CC}_3\text{F}_7)_4$	590 (30)				276 (180)
$\text{Rh}_2(\text{O}_2\text{CCF}_3)_4(\text{Tempo})_2$ (1)	604 (75)	448 (200)			340 (260)
$\text{Rh}_2(\text{O}_2\text{CC}_3\text{F}_7)_4(\text{Tempo})_2$ (2)	600 (146)	440 (400)			396 (400 sh), 344 (420)
$\text{Rh}_2(\text{O}_2\text{CC}_6\text{F}_5)_4(\text{Tempo})_2$ (3)	636 (60)	416 (370)			~408 (360 sh), 332 (550)
Tempo				420 (85)	
$\text{Rh}_2(\text{O}_2\text{CCF}_3)_4(\text{Tempol})_2$ (5)	592 (25)	472 (10)			~304 (280)
$\text{Mo}_2(\text{O}_2\text{CCF}_3)_4(\text{Tempo})_2$ (4)			420 (50)		294 (280)

^aEntries represent λ_{max} values in nm with ϵ values per molecule given in parentheses.

perature down to 4.2 K. Just as for **4**, the data show no signs of short-range or significant long-range order with the straight lines generated from the equation $\chi_M^{-1} = 0.9506T + 0.1380$ with $g = 2.33$. From this Curie-Weiss equation, a Curie constant of 1.052 (emu·K)/mol and a Weiss constant θ of -0.145 K can be calculated.

Electronic Absorption Spectral Data. The visible absorption spectra of $\text{Rh}_2(\text{O}_2\text{CR})_4\text{L}_2$ compounds are known to show pronounced changes as a function of the identity of the coordinating atom of the axial ligand L.²³ The coordinated Tempo complexes **1-3** are all dark green (nearly black) solids, and their solid-state electronic absorption spectra are summarized in Table VIII along with spectral band maxima for **4**, **5**, $\text{Rh}_2(\text{O}_2\text{CC}_3\text{F}_7)_4$, and the Tempo molecule itself. As a result of recent single-crystal polarized electronic spectral studies,³⁸ the low-energy 600-nm and 450-nm bands which are characteristic²³ of $\text{Rh}_2(\text{O}_2\text{CR})_4\text{L}_2$ complexes have been assigned. The Tempo adducts **1-3** show a prominent band around 600 nm that is assigned³⁸ to the $\pi^*(\text{Rh}_2) \rightarrow \sigma^*(\text{Rh-O})$ transition. Additionally, these compounds have another band in the 400-450-nm region with an extinction coefficient that is 2 to 6 times the value found for the low-energy 600-nm-region band. The intensity variation in these extinction coefficients for **1-3** differs from that usually observed. For $\text{Rh}_2(\text{O}_2\text{CC}_3\text{F}_7)_4$, no band in the 450-nm region was resolved. In $\text{Rh}_2(\text{O}_2\text{CCF}_3)_4(\text{Tempol})_2$ (**5**), the bands at 592 and 472 nm have associated extinction coefficients typical of those observed with weak σ -donor axial oxygen ligands.

The orange color of the Tempo ligand is attributed to a weak band around 410-460 nm.³⁹ This band is sensitive to the nitroxyl group environment^{39,40} and assigned to an $n \rightarrow \pi^*$ transition. As shown in Table VIII, the solid state band maximum for this $n \rightarrow \pi^*$ transition in Tempo occurs at 420 nm. Since this band falls within the same region as the $\pi(\text{Rh-O}) \rightarrow \sigma^*(\text{Rh-O})$ transition, it is suggested that excited state interactions between the $\text{Rh}_2(\text{O}_2\text{CR})_4$ and Tempo electronic state manifolds lead to the observed increase in the 400-450-nm region extinction coefficients in the $\text{Rh}_2(\text{O}_2\text{CR})_4(\text{Tempo})_2$ complexes.

Finally, in Table VIII the band maxima for the orange $\text{Mo}_2(\text{O}_2\text{CCF}_3)_4(\text{Tempo})_2$ complex include a band at 420 nm characteristic of the $\delta \rightarrow \delta^*$ transition.^{19,41,42} As noted above, the $n \rightarrow \pi^*$ transition of the nitroxyl group also falls at this same wavelength. However, in contrast to the $\text{Rh}_2(\text{O}_2\text{CR})_4(\text{Tempo})_2$ complexes, the extinction coefficient associated with this 420-nm band is of low intensity. It is entirely possible that the 420-nm band in **4** represents a superposition of $\delta \rightarrow \delta^*$ and $n \rightarrow \pi^*$ transitions in the $\text{Mo}_2(\text{O}_2\text{CCF}_3)_4$ and Tempo electronic state manifolds. Because of the low intensity of this transition, little excited state interactions are suggested; the $\text{Mo}_2(\text{O}_2\text{CCF}_3)_4$ and Tempo chromophores appear to be independent of one another.

Electron Paramagnetic Resonance Spectral Data. EPR spectra (X-band frequencies) were obtained on each of the compounds

1-5 with the samples run as powdered solids and benzene-toluene solutions. The Tempo-coordinated biradicals have EPR spectra at ambient temperatures that consist of a weak asymmetric resonance absorption around $g = 2.00$ with receiver gains of greater than 10^3 . When these biradicals **1-3** are dissolved in benzene-toluene solution, spectra are obtained which suggest an equilibrium mixture of bound mono-Tempo adducts and uncoordinated Tempo radicals.^{25,26} No evidence for a biradical species is present in these EPR solution spectra, suggesting that dissociation of at least one Tempo ligand occurs readily. Therefore, information about the exchange interactions between radical centers must be inferred from the solid-state compounds.

The X-band EPR spectra for powdered samples of $\text{Mo}_2(\text{O}_2\text{CCF}_3)_4(\text{Tempo})_2$ (**4**) and $\text{Rh}_2(\text{O}_2\text{CCF}_3)_4(\text{Tempol})_2$ consist of a single symmetrical absorption with g values of 2.0048 and 2.0054, respectively. Both samples when dissolved in a benzene-toluene solution show typical three-line nitrogen ($I = 1$) hyperfine patterns indicative of the uncoordinated nitroxyl radical.

Powder Diffraction Data. Efforts were made to grow single crystals of $\text{Mo}_2(\text{O}_2\text{CCF}_3)_4(\text{Tempo})_2$ (**4**). Slow diffusion of decane into a benzene solution of **4** always produced a powder while slow evaporation of a benzene solution in an argon-filled drybox yielded noncrystalline green decomposition products. In order to assess the possible similarity between **4** and the crystallographically characterized **1**, powder diffraction patterns were collected on both samples. These patterns are displayed in Figure 3S.³⁶ While the low triclinic symmetry and large number of atoms in the asymmetric unit preclude complete indexing of these patterns, the positions and relative intensities of the diffraction patterns for **1** and **4** suggest that the two compounds may be isomorphous. Isomorphism among $\text{M}_2(\text{O}_2\text{CR})_4\text{L}_2$ compounds is well-documented.⁴³ However, it has been recognized that $\text{Mo}_2(\text{O}_2\text{CCF}_3)_4\text{L}_2$ compounds can exist with not only axial L ligands but also equatorial L ligands of strong σ -donors in which case two of the trifluoroacetate ligands become monodentate.⁴⁴⁻⁴⁸ The infrared spectra for **1** and **4** are also closely similar with no evidence for the monodentate CF_3CO_2^- band around 1670 cm^{-1} .⁴⁵⁻⁴⁷ Weakly σ -donating ligands like Tempo are expected to yield axial adducts with $\text{Mo}_2(\text{O}_2\text{CCF}_3)_4$, and at least one structure ($\text{L} = \text{Et}_2\text{O}$) attests to this bonding pattern.⁴⁹

(43) Representative examples include the following: (a) $\text{R} = \text{CH}_3$, $\text{L} = \text{H}_2\text{O}$, $\text{M} = \text{Cr}$, Rh: Cotton, F. A.; DeBoer, B. G.; LaPrade, M. D.; Pipal, J. R.; Ucko, D. A. *Acta Crystallogr., Sect. B* **1971**, *B27*, 1664-1671. $\text{R} = \text{CH}_3$, $\text{L} = \text{H}_2\text{O}$, $\text{M} = \text{Cu}$: DeMeester, P.; Fletcher, S. R.; Skapski, A. C. *J. Chem. Soc., Dalton Trans.* **1973**, 2575-2578. Brown, G. M.; Chidambaram, R. *Acta Crystallogr., Sect. B* **1973**, *B29*, 2393-2403. (b) $\text{R} = \text{CH}_3$, $\text{L} = \text{pyridine}$ (orthorhombic α form), $\text{M} = \text{Cu}$: Hanic, F.; Stempelova, D.; Hanicova, K. *Acta Crystallogr.* **1964**, *17*, 633-639. $\text{R} = \text{CH}_3$, $\text{L} = \text{pyridine}$ (orthorhombic α form), $\text{M} = \text{Cr}$: Cotton, F. A.; Felthouse, T. R. *Inorg. Chem.* **1980**, *19*, 328-331. (c) $\text{R} = \text{CH}_3$, $\text{L} = \text{pyridine}$ (monoclinic β form), $\text{M} = \text{Cu}$: Barclay, G. A.; Kennard, C. H. L. *J. Chem. Soc.* **1961**, 5244-5251. $\text{R} = \text{CH}_3$, $\text{L} = \text{pyridine}$ (monoclinic β form), $\text{M} = \text{Rh}$: Koh, Y. B.; Christoph, G. G. *Inorg. Chem.* **1978**, *17*, 2590-2596.

(44) Girolami, G. S.; Mainz, V. V.; Andersen, R. A. *Inorg. Chem.* **1980**, *19*, 805-810.

(45) Cotton, F. A.; Lay, D. G. *Inorg. Chem.* **1981**, *20*, 935-940.

(46) Girolami, G. S.; Andersen, R. A. *Inorg. Chem.* **1982**, *21*, 1318-1321.

(47) Santure, D. J.; Sattelberger, A. P. *Inorg. Chem.* **1985**, *24*, 3477-3482.

(48) Spectroscopic data suggest some $\text{Rh}_2(\text{O}_2\text{CCF}_3)_4\text{L}_2$ compounds exist with equatorial L ligands: Telsler, J.; Drago, R. S. *Inorg. Chem.* **1984**, *23*, 2599-2606.

(49) Lay, D. G. Ph.D. Dissertation, Texas A&M University, 1982, pp 16-17, 43-50.

(38) Miskowski, V. M.; Schaefer, W. P.; Sadeghi, B.; Santarsiero, B. D.; Gray, H. B. *Inorg. Chem.* **1984**, *23*, 1154-1162.

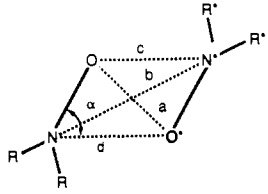
(39) Briere, R.; Lemaire, H.; Rassat, A. *Tetrahedron Lett.* **1964**, 1775-1780.

(40) Janowski, A.; Turowska-Tyrk, I.; Wrona, P. K. *J. Chem. Soc., Perkin Trans. 2* **1985**, 821-825.

(41) Trogler, W. C.; Gray, H. B. *Acc. Chem. Res.* **1978**, *11*, 232-239.

(42) Manning, M. C.; Holland, G. F.; Ellis, D. E.; Trogler, W. C. *J. Phys. Chem.* **1983**, *87*, 3083-3088.

Table IX. Comparison of Solid State Through Space Atomic and Magnetic Interactions between Nitroxyl Groups



compound ^a	R ₂ NO contacts					J, ^b cm ⁻¹	references	
	a, Å	b, Å	c, Å	d, Å	α, deg		structure	magnetic data
A	3.10	3.18	2.86	2.86	88	diamagnetic	51	59
B	2.62	2.62	2.28	2.28	89.9	diamagnetic	52	50, 52
C	3.20	4.61	3.76	3.76	54.9	-93	53	60
D	3.51	4.85	4.03	4.03	57	-23 ^c	54	61
E	3.74	5.09	4.26	4.26	58	-5.6	55	50
F	6.24	5.86	5.02	5.02	126.7	-2.9 ^d	56	60
Tempol	5.84	5.84	4.95	4.95	128.5	-2.9 ^e	57	60
Tempo	5.88	5.88	5.01	5.01	126.6	-1.3 ^f	58 ^g	60
Rh ₂ (O ₂ CCF ₃) ₄ (Tempo) ₂ (1)	4.78	4.97	4.71	4.71	85.7	-239	this work	this work
Rh ₂ (O ₂ CC ₃ F ₇) ₄ (Tempo) ₂ (2)	6.94	6.59	6.10	7.36	65.6	-269	this work	this work

^a For compounds coded with a letter, refer to Chart I in the text. ^b Unless otherwise noted, the Bleaney-Bowers dimer model is assumed. ^c Estimated magnitude from Heisenberg pair model. ^d Estimated magnitude from alternating chain model. ^e Estimated magnitude from linear chain model. ^f Monoclinic polymorph; isomorphous to Tempol.

Discussion

Prior to the inception of this work, a solution EPR study²⁵ of the one-to-one complex formed between Rh₂(O₂CCF₃)₄ and Tempo in toluene reported small shifts in the *g* and *A_N* values of the nitroxyl radical associated with complexation to one of the Rh atoms. A subsequent study²⁶ with Rh₂(O₂CC₃F₇)₄ found even smaller *g* and *A_N* value shifts when an oxygen-, a nitrogen-, a sulfur-, or a carbon-donating atom of a Lewis base L was first coordinated in a one-to-one fashion to give an Rh₂(O₂CC₃F₇)₄L complex and then the Tempo radical allowed to bind to the position trans to the L ligand. These two studies suggest that in solution only a very small amount of nitroxyl spin density is delocalized onto the Rh₂(O₂CR)₄ framework. In contrast, the magnetic susceptibility data reported here show that efficient spin-spin coupling occurs in the solid Tempo biradical complexes 1-3. The key question which must now be addressed for 1-3 is the following: do the observed antiferromagnetic exchange interactions arise from intramolecular (through bond) interactions, intermolecular (through space) interactions, or perhaps a combination of both? The following section considers the available evidence for each of these possibilities.

Through Bond vs. Through Space Interactions. Nitroxyl biradicals are typically examined by using EPR spectroscopy in solution not only to reduce dipolar contributions to the exchange and hyperfine splittings but also to avoid the intermolecular exchange interactions present in the solid state. However, the biradicals 1-3 do not remain intact in solution as evidenced from the solution EPR results described earlier. Therefore, in an effort to assess potential pathways for intermolecular magnetic exchange interactions in 1 and 2, the solid state packing geometries will be examined in detail. For comparison, several nitroxyl radical structures known to exhibit through space magnetic interactions are also considered.

The closest nitroxyl-nitroxyl contacts in Rh₂(O₂CCF₃)₄(Tempo)₂ (1) appear in Figure 7. A stereopacking diagram is displayed in Figure 4S.³⁶ The triclinic crystal structure of 1 results in pairwise contacts of the coordinated Tempo ligands throughout the lattice generated by a combination of inversion plus translation by one unit along the *b* axis. Furthermore, this pairwise nitroxyl-nitroxyl group contacting in 1 occurs with head-to-tail alignments of the N-O bonds and close to the ideal 90° angles (cf. ∠O7T-N1TR...O7T* = 85.7(3)° and ∠O7T-N1TR...N1TR* = 94.3(3)°) at the corners of the (N-O)₂ parallelograms. Since the unpaired electron for each nitroxyl group resides in primarily a π* (antibonding) orbital located parallel to the N-O bond, the orientation of the Tempo nitroxyl groups shown in Figure 7 approaches the optimum for formation of a through-space-

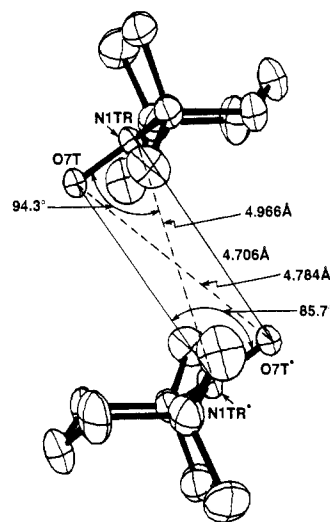


Figure 7. Geometry of the closest intermolecular contacts between Tempo ligands in Rh₂(O₂CCF₃)₄(Tempo)₂.

contacted radical pair. However, the spatial overlap of these π* orbitals at 4.7 to 5.0 Å cannot be expected to produce a singlet-triplet splitting of -478 cm⁻¹ (*J* = -239 cm⁻¹) on the basis of comparisons to several representative through space coupled nitroxyl radical pairs which will now be examined.

The solid-state structures and magnetic properties for a variety of radicals, biradicals, and polyradicals were surveyed by Shibaeva⁵⁰ about a decade ago. Drawings of six representative nitroxyl-containing compounds taken from this survey are shown in Chart I and coded with the letters A through F. Each of these six compounds has been characterized by single-crystal X-ray diffraction⁵¹⁻⁵⁶ and variable-temperature magnetic susceptibility data.^{50,52,59-61} Table IX provides a comparison of the solid-state

(50) Shibaeva, R. N. *Zh. Strukt. Khim.* **1975**, *16*, 330-348; *J. Struct. Chem. (Engl. Transl.)* **1975**, *16*, 318-332.

(51) Howie, R. A.; Glasser, L. S. D.; Moser, W. *J. Chem. Soc. A* **1968**, 3043-3047.

(52) Capiomont, A.; Chion, B.; Lajzerowicz, J. *Acta Crystallogr., Sect. B* **1971**, *B27*, 322-326.

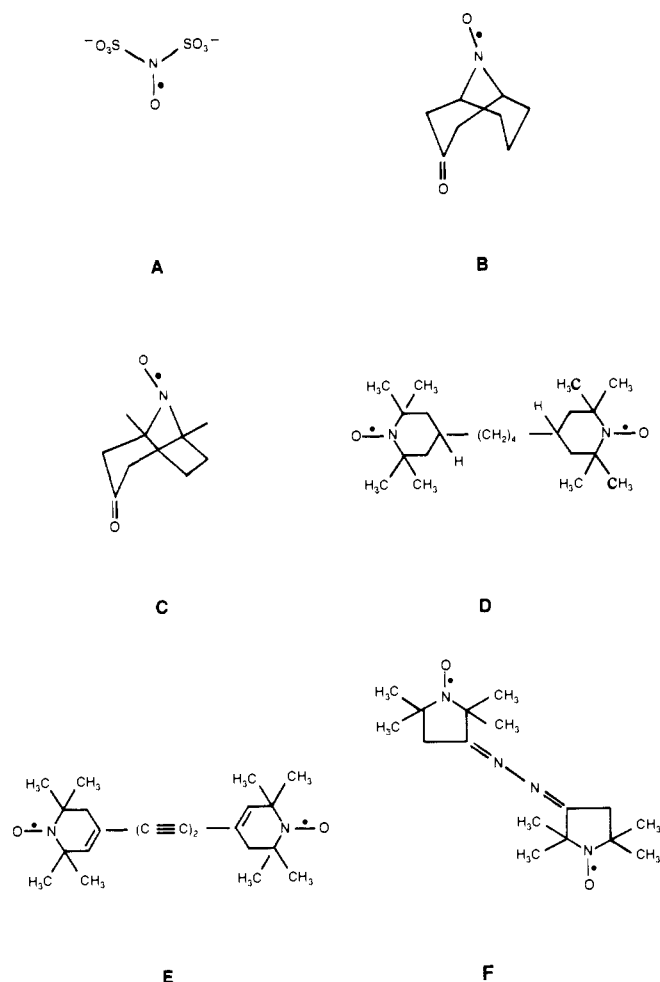
(53) Capiomont, A. *Acta Crystallogr., Sect. B* **1973**, *B29*, 1720-1722.

(54) Shibaeva, R. N.; Rozenberg, L. P. *Zh. Strukt. Khim.* **1974**, *15*, 948-950; *J. Struct. Chem. (Engl. Transl.)* **1974**, *15*, 845-847.

(55) Shibaeva, R. N.; Rozenburg, L. P. *Zh. Strukt. Khim.* **1975**, *16*, 258-261; *J. Struct. Chem. (Engl. Transl.)* **1975**, *16*, 236-239.

(56) Chion, B.; Capiomont, A.; Lajzerowicz, J. *Acta Crystallogr., Sect. B* **1972**, *B28*, 618-619.

Chart 1



nitroxyl-nitroxyl interactions in these six compounds together with data for Tempol,^{57,60} Tempo,^{58,60} **1**, and **2**. As can be seen for compounds A and B, complete radical spin pairing occurs when the nitroxyl groups are oriented in a head-to-tail fashion at less than 3.2 Å. In these compounds the angle α ($\angle\text{O}-\text{N}\cdots\text{O}^*$) approaches 90° in this spin-paired orientation. Compounds C-E contain canted head-to-tail through-space interactions of the nitroxyl groups with α values of 54–58° and N-O separations ranging from 3.2 to 5.1 Å. Antiferromagnetic exchange interactions are observed, are attributed entirely to through-space interactions by means of $\pi^*-\pi^*$ orbital overlaps of the nitroxyl moieties, and are greatly attenuated at these longer distances with singlet-triplet splittings of less than 200 cm⁻¹ in magnitude. Biradical compounds D-F show weak intramolecular through-bond couplings of radical centers detectable by means of solution EPR techniques. For compound F, Tempol, and Tempo in Table IX, the closest nitroxyl-nitroxyl contacts are related by translational symmetry operations, and hence the α values now exceed 90°. The through-space contacts between R₂NO groups can be described as "head-to-head" associations at distances of 4.9 to 6.3 Å. The magnetic behavior for these compounds consists of weak antiferromagnetic exchange interactions that are propagated throughout the crystal lattices and can be fit to various extended chain models.

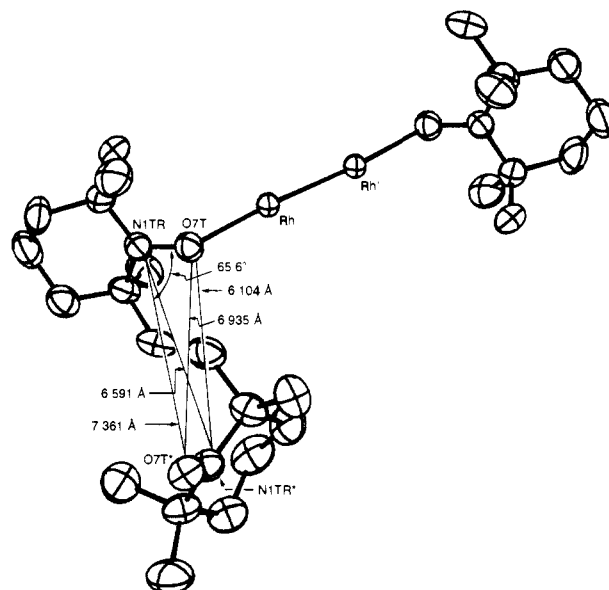


Figure 8. Geometrical orientation of the closest *intermolecular* Tempo ligand to one of the Tempo ligands in Rh₂(O₂CC₃F₇)₄(Tempo)₂ shown with only the Tempo-Rh₂-Tempo atomic framework.

The eight nitroxyl radical containing compounds in Table IX provide a statistical basis for comparisons with the magnetic susceptibility data for **1** and **2**. Thus, while in **1** the possibility exists for through-space interactions in a pairwise fashion, comparison to the eight nitroxyl radical compounds suggests that these exchange interactions would be weaker than -10 cm⁻¹ in **1** due to the 4.7–5.0-Å separation.

The structure of Rh₂(O₂CC₃F₇)₄(Tempo)₂ was undertaken not because any distinct differences in bonding about the dirhodium(II) unit were expected but because with the addition of the bulkier C₃F₇ substituents, *some differences in the intermolecular contacts were anticipated*. In fact, precisely this effect was found in the molecular packing interactions. Figure 8 depicts the closest nitroxyl-nitroxyl contacts relative to the Tempo-Rh₂-Tempo unit. A complete view of the molecular packing within the unit cell appears in a stereopacking diagram in Figure 5S.³⁶ The monoclinic space group in **2** generates an infinite zigzag stacking of the closest N-O bonds of the Tempo ligands at 6.1–7.4 Å (cf., the increase in these stacking distances to the 4.7–5.0-Å separations in **1**) by means of the *c*-glide plane. As seen in Figures 5S³⁶ and 8, the R₂NO contacts are canted with an α value (Table IX) of 65.6°. This zigzag contacting no longer is near the optimum of 90° (= $\angle\text{O}-\text{N}\cdots\text{O}^*$) required for $\pi^*-\pi^*$ orbital overlaps. If through-space interactions between these closest nitroxyl groups in **2** were important to the observed magnetic susceptibility data, structure **2** would require a one-dimensional chain model. Through-space coupled radical pairs listed in Table IX offer *no support* to the hypothesis that an exchange interaction on the order of -269 cm⁻¹ will arise between nitroxyl π^* orbitals located at more than 6.1 Å. The strong spin pairing observed in the magnetic susceptibility data for **2** is not characteristic of long-range interactions (for examples see ref 62) that would be present in **2** if through-space coupling occurred. The inescapable conclusion to be drawn from the data in Table IX is that **1** and **2** have magnetic behavior that is not accounted for by significant through-space interactions between nitroxyl groups but arises entirely from an intramolecular through-bond coupling by way of the Rh₂(O₂CR)₄ bridging groups. The magnetic susceptibility data for **1–3** are well-fit by the Bleaney-Bowers equation, and because of the strong antiferromagnetic couplings any *intermolecular* interactions which might be expected from the packing interactions will not be observed since biradicals **1–3** are essentially diamagnetic at low (<80 K) temperatures.

(57) Berliner, L. J. *Acta Crystallogr., Sect. B* **1970**, B26, 1198–1202.

(58) Capiomont, A.; Lajžerowicz-Bonneteau, J. *Acta Crystallogr., Sect. B* **1974**, B30, 2160–2166.

(59) Moser, W.; Howie, R. A. *J. Chem. Soc. A* **1968**, 3039–3043.

(60) Veyret, C.; Blaise, A. *Mol. Phys.* **1973**, 25, 873–882.

(61) Zvarykina, A. V.; Stryukov, V. B.; Umanskii, S. Ya.; Fedutin, D. N.; Shibaeva, R. N.; Rozantsev, E. G. *Dokl. Akad. Nauk SSSR* **1974**, 216, 1091–1094; *Bull. Acad. Sci. USSR, Phys. Chem. (Engl. Transl.)* **1974**, 216, 555–557.

(62) Carlin, R. L. *Magnetochemistry*; Springer-Verlag: Berlin, 1986; Chapters 5–7.

Table X. Summary of Structural and Magnetic Data for $M_2(O_2CR)_4L_2$ Compounds

M	R	L	M-M, Å	M-L, Å	M-O _{eq} , ^a Å	O-C, ^a Å	bridge length, ^b Å	J, cm ⁻¹	references	
									structure	χ_M data
Rh	CF ₃	Tempo	2.417 (1)	2.220 (2)	2.032 (2)	1.248 (4)	6.857 (11.000) ^c	-239	this work	this work
Rh	C ₃ F ₇	Tempo	2.431 (1)	2.235 (5)	2.036 (5)	1.245 (9)	6.901 (11.032) ^c	-269	this work	this work
Rh	CF ₃	Tempol ^d	2.405 (1)	2.240 (3)	2.034 (2)	1.250 (5)	18.799 ^e	<0.5	27	this work
Cu	CH ₃	H ₂ O	2.614 (2)	2.161 (2)	1.969 (2)	1.259 (2)	6.456	-143	63	37, 64
Cu	CF ₃	quinoline	2.886 (2)	2.107 (6)	1.972 (6)	1.242 (11)	6.41	-155	66	66

^a Mean distance. ^b Mean distance between paramagnetic centers defined as M-O-C-O-M except where noted. ^c Mean through-bond distances: O_L-Rh-Rh-O_L (O_L-Rh-O-C-O-Rh-O_L) where O_L is the axial nitroxyl O atom. ^d Coordinated through hydroxyl oxygen atoms. ^e Mean through-bond distance: N-C-C-C-O-Rh-Rh-O-C-C-C-N.

Table XI. Nitroxyl Group Bonding

compound	M-O, Å	M-O-N, deg	N-O, Å	C-N-C, deg	α , ^a deg	reference
Rh ₂ (O ₂ CCF ₃) ₄ (Tempo) ₂	2.220 (2)	138.0 (1)	1.275 (3)	123.9 (3)	3.0	this work
Rh ₂ (O ₂ CC ₃ F ₇) ₄ (Tempo) ₂	2.235 (5)	134.2 (4)	1.288 (7)	125.4 (5)	6.5	this work
Tempo			1.296 (5)	125.5 (3)	19.4	58
Cu(hfac) ₂ (Tempo)	1.920 (5)	123.9 (4)	1.269 (7)	124.3 (7)	27.6	71
Cu ₂ (O ₂ CCl ₃) ₄ (Tempo) ₂ ^b	1.942 (8), 1.950 (8)	123.5 (7), 123.9 (7)	1.278 (12), 1.296 (12)	125.0 (11), 125.2 (10)	15.3, 14.1	16
Rh ₂ (O ₂ CCF ₃) ₄ (Tempol) ₂	2.01 (4) ^c	120 (1) ^c	1.282 (4)	125.2 (3)	18.6	27
Tempol			1.291 (7)	125.4 (5)	15.8	57
Cu(hfac) ₂ (Tempol)	2.439 (6)	170.1 (5)	1.276 (8)	126.7 (6)	5.2	72
CuC ₃₂ H ₅₄ N ₂ O ₈ ^{b,d}	2.583 (5), 3.157 (5)	158.5 (4), 139.5 (4)	1.283 (5), 1.261 (6)	124.7 (4), 124.2 (5)	19.3, 21.8	73

^a Out-of-plane acute angle between the N-O bond and the C-N-C plane. ^b This molecule contains two inequivalent nitroxyl groups. ^c Hydrogen-bonded contact: M = H. ^d Formula for bis[(1-oxy-2,2,6,6-tetramethylpiperidin-4-yl)pivaloylaceta]copper(II).

If the above structural comparisons serve to support the notion of through-bond couplings in 1-3, then the observed magnetic behavior for 4 and 5 certainly provides further evidence that through-space interactions are insignificant in $M_2(O_2CR)_4$ -biradical compounds. Although the detailed structure for $Mo_2(O_2CCF_3)_4(Tempol)_2$ is not known, powder diffraction data presented here in conjunction with analogous structures with weak axial oxygen σ -donor ligands⁴⁹ suggest that if this compound adopts similar nitroxyl-nitroxyl contacts to those in 1, an opportunity exists for some through-space interactions albeit at a long (ca. 5-7 Å) distance. However, the magnetic data for 4 are well-fit to the Curie-Weiss equation implying that $|J| < 0.5 \text{ cm}^{-1}$.

The magnetic susceptibility data for $Rh_2(O_2CCF_3)_4(Tempol)_2$ (5) also show Curie-Weiss behavior down to 4.2 K. The detailed structure has been reported²⁷ and shows an intramolecular through-bond separation of the nitroxyl groups of about 18.8 Å. A planar projection of the unit cell contents for 5 appears in Figure 6S.³⁶ Much closer intermolecular nitroxyl contacts exist, but these through-space interactions are still greater than ca. 6.4 Å (O6'...O6* in Figure 6S³⁶). In 5 no viable pathway exists for effective spin coupling between nitroxyl groups and no interaction (e.g., $|J| < 0.5 \text{ cm}^{-1}$) is observed.

Comparisons to $Cu_2(O_2CR)_4L_2$ Compounds. The above detailed analysis of the crystal structures of 1 and 2 provides compelling evidence that the strong antiferromagnetic spin coupling in 1-3 arises solely from an intramolecular through-bond interaction involving the $Rh_2(O_2CR)_4$ framework. Despite numerous prior studies involving metal-nitroxyl interactions (typically using a paramagnetic metal ion), compounds 1-3 represent the first examples in which a magnetic exchange interaction is propagated by a metal-metal bonded complex. The tetrakis(carboxylato)-dimetal(II) framework has been historically linked to studies on both strong^{19,20} and weak metal-metal bonding interactions. Among the "weak" metal-metal bonded compounds, none has been more thoroughly investigated than the copper(II) acetate hydrate dimer^{37,63,64} which formally contains no Cu-Cu bond. Molecular mechanics calculations on $M_2(O_2CR)_4L_2$ systems find that the M-M distances in Rh_2^{4+} and Cu_2^{4+} complexes are sterically compressed by the bridging carboxylato groups.⁶⁵ Table X collects some structural and magnetic data on $Cu_2(O_2CCH_3)_4(H_2O)_2$, a related trifluoroacetate Cu_2^{4+} complex with axial quinoline lig-

ands,⁶⁶ and three Rh_2^{4+} complexes reported here.

Perusal of Table X structural data shows that while the Rh_2^{4+} complexes contain an M-M separation shorter by ca. 0.2 Å than the Cu_2^{4+} complexes, the distance between paramagnetic centers is at least 0.5 Å shorter for the two $Cu_2(O_2CR)_4L_2$ complexes. Recent theoretical studies⁶⁷ on $Cu_2(O_2CCH_3)_4(H_2O)_2$ support the absence of any Cu-Cu "δ" bond and a superexchange pathway involving the copper $d_{x^2-y^2}$ orbitals and the acetate ligands. Thus, the unpaired electron on each copper(II) ion must be delocalized across only the carboxylate bridges in order to give rise to the exchange couplings of -143 to -155 cm⁻¹. On the other hand, the two Rh_2^{4+} complexes in Table X with Tempo axial ligands have an unpaired electron in each nitroxyl π^* orbital parallel to the N-O bond. Through-bond separations between unpaired electrons in 1 and 2 assuming that the unpaired spin density is located at each nitroxyl oxygen atom are found to be at least 6.8 Å and perhaps as long as 11 Å if the analogous carboxylato bridging pathway is chosen for these Rh_2^{4+} complexes as it was for the Cu_2^{4+} complexes. The remarkable point to note is that the exchange interactions, as gauged by the exchange parameter J, in 1 and 2 are nearly double in magnitude to the values found in the $Cu_2(O_2CR)_4L_2$ complexes. The factors that contribute to this efficient spin coupling across the $Rh_2(O_2CR)_4$ framework will be examined shortly.

Coordinated Nitroxyl Group Bonding. The first examples of the nitroxyl group used as a coordinating ligand to a metal ion appeared in 1967 when a series of $Co[ON(CMe_3)_2]_2X_2$ complexes with X = Cl, Br, I was prepared.⁶⁸ However, only recently have structural data provided quantitative details on coordinated nitroxyl groups. In two instances with Pd(II) complexes, the Tempo ligand has been found to coordinate in a π -bonded η^2 -N-O fashion, but here the nitroxyl group has undergone a one-electron reduction.^{69,70} In all other examples encountered to date, the nitroxyl group has been found to coordinate through one of the two lone pairs on the oxygen atom in σ -bonded fashion.

Although compounds 1 and 2 are the first structurally characterized examples of nitroxyl group coordination to rhodium, the

(66) Moreland, J. A.; Doedens, R. J. *J. Am. Chem. Soc.* **1975**, *97*, 508-513.

(67) DeLoth, P.; Cassoux, P.; Daudey, J. P.; Malrieu, J. P. *J. Am. Chem. Soc.* **1981**, *103*, 4007-4016.

(68) Beck, W.; Schmidtner, K.; Keller, H. *J. Chem. Ber.* **1967**, *100*, 503-511.

(69) Dickman, M. H.; Doedens, R. J. *Inorg. Chem.* **1982**, *21*, 682-684.

(70) Porter, L. C.; Doedens, R. J. *Acta Crystallogr., Sect. C* **1985**, *C41*, 838-840.

(63) See ref 43a with M = Cu.

(64) Figgis, B. N.; Martin, R. L. *J. Chem. Soc.* **1956**, 3837-3846.

(65) Boeyens, J. C. A.; Cotton, F. A.; Han, S. *Inorg. Chem.* **1985**, *24*, 1750-1753.

Rh–O(nitroxyl) distances of ca. 2.2 Å and the Rh–O–N angles of 134–138° agree well with a σ -bonded model for the Tempo nitroxyl ligands. Table XI assembles pertinent structural parameters for the nitroxyl group bonding in **1**, **2**, and several other compounds containing the 2,2,6,6-tetramethylpiperidinyl-1-oxyl ring.^{16,27,57,58,71–73} As the data in Table XI show, nitroxyl group coordination to the Rh atoms in **1** and **2** produces no detectable effect on the N–O bond length which remains in the 1.26–1.30-Å range expected for a bond order of 1.5. The C–N–C angles of 123.9 (3) and 125.4 (5)° for **1** and **2**, respectively, are in accord with the range of values represented here for piperidine-based nitroxides. The nitroxyl group conformation as defined by the angle α in Table XI is nearly planar in **1** and **2** with angles of 3.0 and 6.5°, respectively. With the exception of Cu(hfac)₂(Tempo),⁷² the other C₂NO groups represented in Table XI adopt distinctly pyramidal geometries with α values above 14°. However, it appears that neither the planar nor pyramidal form of the C₂NO groups is strongly favored.

Perhaps the key structural parameters that relate to the observed magnetic properties of the compounds in Table XI having coordinated nitroxyl groups are the M–O(nitroxyl) bond lengths and the M–O–N angles. For the six compounds in Table XI with coordinated nitroxyl groups, the M–O bond lengths in fact conveniently group these compounds into three classes, each with a characteristic magnetic behavior.

The shortest M–O(nitroxyl) bonds are found in Cu(hfac)₂(Tempo)⁷¹ and Cu₂(O₂CCCl₃)₄(Tempo)₂¹⁶ and both molecules show strong intramolecular antiferromagnetic spin coupling.^{16,74} This coupling is accounted for by the favorable overlap of the nitroxyl π^* orbital with either the $d_{x^2-y^2}$ or d_{z^2} orbitals in Cu(hfac)₂(Tempo) (the Cu geometry is intermediate between square pyramidal and trigonal bipyramidal) or the d_{z^2} -torus orbitals in Cu₂(O₂CCCl₃)₄(Tempo)₂. In contrast, a second class of copper(II)-nitroxide complexes shown in Table XI exhibits uniquely weak ferromagnetic exchange interactions characterized by long Cu–O(nitroxyl) bond lengths and a strong angular dependence⁷³ to the exchange interaction. For Cu(hfac)₂(Tempo)⁷² the observed magnetic behavior^{75,76} is interpreted in terms of an alternating chain model⁷⁶ with a net ferromagnetic coupling between Cu–nitroxide pairs ($J = +26 \text{ cm}^{-1}$) along an infinite chain which gives rise to weak ($J' = -0.11 \text{ cm}^{-1}$) antiferromagnetic coupling between the ferromagnetic Cu–nitroxide pairs. Here the ferromagnetic interaction is due to the near orthogonality of the copper d_{xy} orbital with the nitroxyl π^* orbital.⁷⁵ A similar analysis explains the net ferromagnetic exchange interaction ($J = +9.6 \text{ cm}^{-1}$) between the copper–nitroxide magnetic orbitals in CuC₃₂H₅₄N₂O₈ listed in Table XI.

The third class of compounds represented in Table XI comprises the Rh₂(O₂CR)₄-bridged biradicals **1** and **2**. The nitroxyl groups coordinate to the metal centers at distances (ca. 2.2 Å) intermediate between either of the copper(II)-nitroxide classes that show short (<2 Å) and long (2.5–3.2 Å) metal–O(nitroxyl) bond lengths. Coincidentally, the M–O–N angles fall between the two classes of copper–nitroxide compounds. However, a strict analogy in the magnetic behavior of **1** and **2** cannot be made with the copper(II)-nitroxides because the nitroxyl π^* magnetic orbital does not bond directly with the atom containing the second unpaired electron but rather must rely on spin delocalization over the Rh₂(O₂CR)₄ frameworks. Additionally, metal–metal bonded compounds in general give rise to different orbital configurations than are possible with mononuclear metal atoms. The next section illustrates this point for the Rh₂(O₂CR)₄(Tempo)₂ compounds reported here.

Exchange Mechanism. Over the past several years the factors

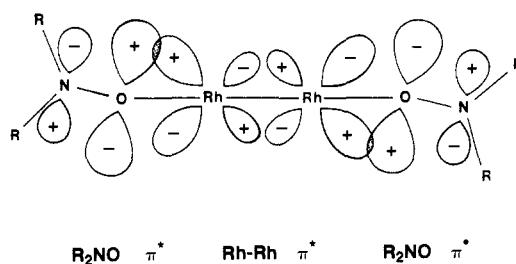


Figure 9. Principal superexchange pathway for the Rh₂(O₂CR)₄(Tempo)₂ molecules showing the effective overlap of the Rh–Rh π^* and R₂NO π^* orbitals.

important to the design and construction of effective multiatomic bridging units that propagate exchange interactions between paramagnetic sites have begun to emerge.^{22,77–79} While ab initio SCF–MO calculations⁶⁷ offer a rigorous means to determine the singlet–triplet (ST) energy splitting as a function of the molecular orbitals in the complex, a qualitative analysis explains how such a large ST splitting can arise in **1**–**3**. Two key factors determine the ST energy splitting in the Rh₂(O₂CR)₄(Tempo)₂ complexes: (1) the orbital overlap between the nitroxyl p_{π^*} orbitals containing the unpaired electrons and the appropriate Rh₂(O₂CR)₄ orbitals and (2) the energy difference between the p_{π^*} orbitals and the exchange-propagating orbitals of Rh₂(O₂CR)₄.

Since the electronic structures of both the nitroxyl R₂NO⁶⁸ and Rh₂(O₂CR)₄L₂^{80–82} fragments are known, the interactions between orbitals can be well-defined. The SCF–X α –SW calculations⁸⁰ on Rh₂(O₂CH)₄(H₂O)₂ reveal that the order of primarily Rh–Rh hybridized d orbitals is $\pi^4\sigma^2\delta^2\pi^*4\delta^*2$. Electronic spectra for **1**–**3** show bands in essentially the same region as Rh₂(O₂CR)₄(H₂O)₂. The addition of the electron-withdrawing CF₃, C₃F₇, or C₆F₅ substituents is expected to cause a uniform downshifting of the Rh₂(O₂CR)₄L₂ orbitals, and this is manifested by a stronger Rh–O(axial) interaction. The Rh–O distance decreases from 2.310 (3) Å in Rh₂(O₂CCH₃)₄(H₂O)₂^{43a} to 2.243 (2) Å in Rh₂(O₂CCF₃)₄(H₂O)₂[ON(CMe₃)₂]₂.²⁷ However, some elongation of the Rh–Rh bond is observed since the axial H₂O ligands bind more tightly. Overall, one expects the basic ordering of Rh–Rh d orbitals to be well-represented by the X α –SW calculations⁸⁰ on Rh₂(O₂CH)₄(H₂O)₂.

The bonding interaction between the nitroxyl oxygen atoms with the Rh atoms in **1**–**3** is comprised of two components. The nitroxyl oxygen lone pair donation to the Rh results in the axial Rh–O bond which is strengthened by the presence of the electron-withdrawing fluorine atoms on the carboxyl R group substituents. The Rh₂(O₂CR)₄ framework concentrates electron density in antibonding orbitals which provide the second means by which the Rh₂(O₂CR)₄ nucleus can interact with incoming axial ligands. The nitroxyl p_{π^*} orbitals containing the unpaired electrons will interact most effectively with the highest filled Rh₂ orbitals. The δ^* orbitals within the Rh₂(O₂CR)₄ manifold represent the HOMO but are of incorrect symmetry to interact with the p_{π^*} orbitals. However, the next highest filled orbitals of the Rh₂(O₂CR)₄ framework are the Rh₂ π^* which are precisely of the correct symmetry to overlap effectively with the incoming nitroxyl p_{π^*} orbitals. This Rh₂ π^* – p_{π^*} overlap is depicted in Figure 9, and the effectiveness of the overlap will depend on the energy difference between these π^* orbitals. Thus, the Rh–O(nitroxyl) bonding is characterized by an Rh–O σ bond and a π -back-bonding between the Rh₂ π^* and the nitroxyl p_{π^*} orbital.

(77) Hay, P. J.; Thibeault, J. C.; Hoffmann, R. *J. Am. Chem. Soc.* **1975**, *97*, 4884–4899.

(78) Kahn, O. *Inorg. Chim. Acta* **1982**, *62*, 3–14.

(79) Kahn, O. *Angew. Chem., Int. Ed. Engl.* **1985**, *24*, 834–850.

(80) Norman, J. G., Jr.; Kolari, H. J. *J. Am. Chem. Soc.* **1978**, *100*, 791–799.

(81) Norman, J. G., Jr.; Renzoni, G. E.; Case, D. A. *J. Am. Chem. Soc.* **1979**, *101*, 5256–5267.

(82) Christoph, G. G.; Koh, Y.-B. *J. Am. Chem. Soc.* **1979**, *101*, 1422–1434.

(71) Dickman, M. H.; Doedens, R. *J. Inorg. Chem.* **1981**, *20*, 2677–2681.

(72) Anderson, O. P.; Kuechler, T. C. *Inorg. Chem.* **1980**, *19*, 1417–1422.

(73) Grand, A.; Rey, P.; Subra, R. *Inorg. Chem.* **1983**, *22*, 391–394.

(74) Lim, Y. Y.; Drago, R. S. *Inorg. Chem.* **1972**, *11*, 1334–1338.

(75) Bencini, A.; Benelli, C.; Gatteschi, D.; Zanchini, C. *J. Am. Chem. Soc.* **1984**, *106*, 5813–5818.

(76) Benelli, C.; Gatteschi, D.; Carnegie, D. W., Jr.; Carlin, R. L. *J. Am. Chem. Soc.* **1985**, *107*, 2560–2561.

As can be seen in Figure 9, the $Rh_2\pi^*$ orbital alone does not provide a continuous bonding framework over which the exchange interaction can be propagated between nitroxyl groups. However, as the $X\alpha$ -SW calculations on $Rh_2(O_2CH)_4(H_2O)_2$ show,⁸⁰ the $Rh_2\pi^*$ orbital is actually composed of only ca. 80% Rh_2 with the remaining contributions due to a mixture of carboxylate and water (or nitroxide) orbitals. As the symmetry of the complex is reduced from D_{2h} , admixture of the $Rh_2\pi^*$ orbitals with the $Rh_2\pi$ and $Rh_2\sigma$ can occur through configuration interactions with excited states. It appears that once an effective overlap is made with the $Rh_2(O_2CR)_4$ framework, many pathways exist to propagate the interaction, and this is certainly aided by the relatively close energetic proximity of the 14 primarily Rh_2 electrons available in the $\pi^4\sigma^2\delta^2\pi^*2\delta^*2$ manifold.

Previous extended Hückel overlap calculations⁷³ on the interaction between the p_π^* orbital on a nitroxide ligand and the d_{xy} magnetic orbital (i.e., the orbital containing the unpaired electron) on a mononuclear copper(II) complex have predicted a strong angular dependence to the exchange interaction. In fact, the data presented in Table XI in conjunction with earlier discussion corroborate these calculational results. Since the $Rh_2\pi^*$ orbital is comprised of contributions from d_{xz}^* and d_{yz}^* , the resulting orbital unlike the Cu d_{xz} orbital maps out a three-dimensional surface and not just a two-dimensional plane. The interaction of the $Rh_2\pi^*$ surface with the planar p_π^* nitroxyl orbital, therefore, is expected *not* to be strongly angle dependent. Instead the Rh-O(nitroxyl) distance is expected to contribute strongly to the $Rh_2\pi^*-p_\pi^*$ overlap.

Comparison of the exchange parameters for 1-3 suggests some differences due to the R group substituent. The structures of 1 and 2 are closely similar as are the J values for these compounds (-239 and -269 cm^{-1} , respectively). However, when $R = C_6F_5$ in 3 the exchange parameter drops to -184 cm^{-1} . In the absence of structural data, it is not possible to tell if this is due to some difference in the Rh-O(nitroxyl) bonding. In this abbreviated series of $Rh_2(O_2CR)_4(Tempo)_2$ complexes, subtle electronic effects of the R group substituent may play a role which at this point cannot be fully appreciated.

The ST splittings of -368 to -538 cm^{-1} in 1-3 arise as a consequence of the effective $Rh_2\pi^*$ back-bonding into the nitroxyl p_π^* orbitals. The existence of extensive π -back-bonding capabilities in $Rh_2(O_2CR)_4L_2$ complexes has been proposed^{83,84} for some time. For some axial donor ligands such as phosphines, the π -back-bonding arguments have been challenged⁸⁵ with support through $X\alpha$ -SW calculations⁸⁵ and EPR data.⁸⁶ The strong antiferromagnetic exchange interactions observed in 1-3 provide direct experimental evidence for π back-bonding, but this assertion requires some qualifications. The $X\alpha$ -SW calculations⁸⁰ support this view in terms of the basic electronic structure in $Rh_2(O_2CR)_4L_2$ complexes with axial oxygen donor ligands. Magnetic exchange interactions represent an extraordinarily weak form of chemical bonding. Ab initio SCF-MO calculations⁶⁷ on $Cu_2(O_2CCH_3)_4(H_2O)_2$ find that a high degree of configuration interaction is required to obtain a meaningful *estimate* of the ST energy gap. The presence or absence of these exchange interactions in a complex cannot be measured in terms of bond distance changes. No effect is seen on the N-O bond distance upon coordination to the $Rh_2(O_2CR)_4$ framework in 1 or 2. The expected Rh-Rh bond shortening as a result of π^* back-donation into the half-filled nitroxyl p_π^* orbital is not observed, and on the contrary, the Rh-Rh bond is seen to lengthen. Similar effects are observed in $Rh_2(O_2CCH_3)_4(CO)_2$,⁸⁷ so even with a good

π -acceptor ligand like CO, it appears that the mutual σ trans effect on the Rh-Rh and Rh-L(axial) bonding predominates in the bonding description.

Reference to $X\alpha$ -SW calculations on $Mo_2(O_2CH)_4$,^{80,88} affords an explanation for the lack of any exchange interaction in $Mo_2(O_2CCF_3)_4(Tempo)_2$ (4). As pointed out before, one expects a very long Mo-O(nitroxyl) distance, probably greater than 2.5 Å by comparison with $Mo_2(O_2CCF_3)_4(Et_2O)_2$.⁴⁹ The $\sigma^2\pi^4\delta^2$ orbitals of Mo_2^{4+} all participate in the formation of the quadruple bond, and no additional metal-based orbitals are available for axial bonding. Indeed, the axial adducts of $Mo_2(O_2CCF_3)_4$ are found to be thermally labile and incapable of all but weak σ -donation to the Mo centers. The lack of filled $Mo_2\pi^*$ orbitals precludes any $M_2\pi^*$ back-bonding in $Mo(O_2CCF_3)_4(Tempo)_2$ that is so effective in the exchange mechanism for the $Rh_2(O_2CR)_4(Tempo)_2$ compounds.

The Distance Dependence Limit Function. Several years ago a statistical analysis of magnetic exchange interactions was performed for $S_1 = S_2 = 1/2$ spin systems in which a plot of $\log J$ vs. distance R was constructed.⁸⁹ From this analysis, a limit function was proposed which for an exchange Hamiltonian of the form $\hat{H} = -2J\hat{S}_1\hat{S}_2$, the function can be expressed as shown in eq 3. In this equation, R is expressed in Å and J is given in cm^{-1} .

$$J = (-6.75 \times 10^6) \exp(-1.80R) \quad (3)$$

Thus, for a given distance R between paramagnetic centers having spins of S_1 and S_2 , the magnetic exchange interaction is predicted to be less than the value of J calculated from eq 3. A few years ago it was noted⁹⁰ that certain organic biradicals such as those depicted by G and H⁹¹ below exhibit $|J|$ values that exceed prediction by eq 3. Additionally, at the time the limit function was proposed, the paucity of systems having distances between paramagnetic centers greater than 6 Å was acknowledged. The biradicals 1 and 2 in this work now provide additional violations to the statistical limit function in eq 3.

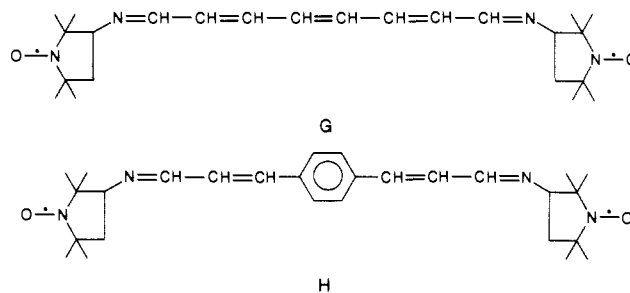


Table XII accumulates data for some eight "violators"⁹¹⁻⁹⁵ to the distance dependence limit function arranged in order of increasing distance R between the spin $1/2$ centers. All four of the binuclear Cu(II) complexes interact by way of σ -based spin delocalization. The first two copper complexes contain in essence the dithioxamide bridging unit. The remaining four compounds are biradicals (1, 2, G, and H), and these appear to propagate spin density primarily by way of π systems. Because of the delocalized electron in the π^* orbital of the nitroxyl group, an exact distance cannot be given, but a through-space separation range is listed. For these four biradicals, even the shortest distance R between radical centers produces substantial deviation from the observed J value. These studies⁹⁰⁻⁹⁵ clearly point out that a simple distance dependence cannot be predicted for long-range (>5 Å) magnetic-exchange interactions. The dirhodium(II) cluster complexes

(83) Drago, R. S.; Tanner, S. P.; Richman, R. M.; Long, J. R. *J. Am. Chem. Soc.* **1979**, *101*, 2897-2903.

(84) Drago, R. S.; Long, J. R.; Cosmano, R. *Inorg. Chem.* **1981**, *20*, 2920-2927.

(85) Bursten, B. E.; Cotton, F. A. *Inorg. Chem.* **1981**, *20*, 3042-3048.

(86) Kawamura, T.; Fukamachi, K.; Sowa, T.; Hayashida, S.; Yonezawa, T. *J. Am. Chem. Soc.* **1981**, *103*, 364-369.

(87) Koh, Y.-B. Ph.D. Thesis, The Ohio State University, 1979. Reference 85, footnote 37, provides comments on the π -back-bonding interaction in $Rh_2(O_2CCH_3)_4(CO)_2$.

(88) Norman, J. G., Jr.; Kolari, H. J.; Gray, H. B.; Trogler, W. C. *Inorg. Chem.* **1977**, *16*, 987-993.

(89) Coffman, R. E.; Buettner, G. R. *J. Phys. Chem.* **1979**, *83*, 2387-2392.

(90) Francesconi, L. C.; Corbin, D. R.; Clauss, A. W.; Hendrickson, D. N.; Stucky, G. D. *Inorg. Chem.* **1981**, *20*, 2059-2069.

(91) Shapiro, A. B.; Norozhilova, G. A.; Dombrovskii, V. A.; Volodarskii, L. B.; Rozantsev, E. G. *Izv. Akad. Nauk SSSR, Ser. Khim* **1976**, 2124-2127; *Bull. Acad. Sci. USSR, Div. Chem. Sci. (Engl. Transl.)* **1976**, 1988-1991.

Table XII. Violations of the Limit Function^a for Magnetic Exchange Interactions

compound ^b	<i>R</i> , Å	<i>J</i> , cm ⁻¹		reference
		predicted ^d	observed	
{Cu ₂ [S ₂ C ₂ (NCH ₂ CH ₂ OH) ₂](H ₂ O) ₂]SO ₄ }	5.61	-278	-297	92
Cu ₂ DT(metOMe) ₂ Br ₂	5.666	-251	-365	93
Rh ₂ (O ₂ CCF ₃) ₄ (Tempo) ₂ (1)	6.853–8.948	-29.7 to -0.68	-239	this work
Rh ₂ (O ₂ CC ₃ F ₇) ₄ (Tempo) ₂ (2)	6.896–8.913	-27.4 to -0.73	-269	this work
Cu ₂ A ₂ (CH ₃ CO ₂) ₂	9.097	-0.52	-1.33	94
{Cu ₂ (tren) ₂ (BZD)}(NO ₃) ₄	12.273, 12.083	-0.0017, -0.0024	-4.5	95
biradical G	20–24 ^e	-1.6 × 10 ⁻⁹ to -1.2 × 10 ⁻¹²	0.0013 ^f	91
biradical H	23–28 ^e	-7.1 × 10 ⁻¹² to -8.7 × 10 ⁻¹⁶	0.00035 ^f	91

^aLimit function as defined in text, eq 3. ^bAbbreviations defined in text except as follows: DT(metOMe)₂ = {C₂S₂[NCH(CH₂CH₂SCH₃)COO-CH₃]₂}; A = anion of *N*-methyl-*N'*-salicylidene-1,3-propanediamine; tren = 2,2',2''-triaminotriethylamine; and BZD = benzidine (*p*-diaminodiphenyl). ^cDistance between unpaired spin density. ^dAccording to *R* value given and eq 3, assuming $\hat{H} = -2J\hat{S}_1\hat{S}_2$. ^eEstimated from CPK models. ^fObtained from EPR spectrum; only the relative magnitude is known.

described here provide a novel way to propagate long-range interactions, and such a methodology should be applicable to other cluster systems.

Conclusions

This investigation represents the first study to examine the ability of metal–metal bonded complexes to propagate a magnetic exchange interaction. Strong intramolecular through-bond coupling occurs in the Rh₂(O₂CR)₄(Tempo)₂ compounds for R = CF₃, C₃F₇, and C₆F₅. Magnetic susceptibility data on powdered samples of these dirhodium(II) compounds are well-fit to a simple $S_1 = S_2 = 1/2$ spin coupling model (the Bleaney–Bowers equation). Detailed comparisons of the intermolecular interactions in the solid Rh₂(O₂CR)₄(Tempo)₂ structures (R = CF₃, C₃F₇) with interactions found in the structures of solid-state nitroxyl radicals suggest *no appreciable through-space interactions occur in the dirhodium–biradical compounds*. The biradical complex Mo₂(O₂CCF₃)₄(Tempo)₂ containing quadruply bonded dimolybdenum(II) was prepared and found to show Curie–Weiss behavior in the solid-state magnetic susceptibility data. The magnetic susceptibility data for these dimetal–biradical compounds are well-interpreted in terms of accepted ground-state electronic structures of M₂(O₂CR)₄ and the nitroxyl radical groups. The exchange mechanism in the Rh₂(O₂CR)₄(Tempo)₂ compounds is explicable in terms of an Rh₂π*–(Tempo)_{π*} back-bonding model. The absence of filled π* orbitals in Mo₂(O₂CCF₃)₄ precludes a π*–back-bonding interaction with the nitroxyl π* orbitals,

and no interaction between nitroxyl centers is observed.

The dirhodium(II)–biradical compounds show through-bond coupling that exceeds that found in the classic tetrakis(carboxylato)copper(II) compounds in which the unpaired electrons reside in metal-based orbitals. However, these dicopper(II) compounds lack genuine metal–metal bonds, are complicated by the addition of nitroxyl groups since extraction of the individual spin–spin couplings (i.e., radical–radical) is not straightforward, and show severe geometrical distortions from the classic dimetal–tetra-carboxylate framework when axial ligands are introduced. The magnitude of the magnetic exchange interactions found in the Rh₂(O₂CR)₄(Tempo)₂ compounds actually exceeds that calculated from a statistically based relationship between the exchange parameter and the spin–spin separation. The exchange interaction is not related adequately by this simple distance dependence limit function, and several examples including those provided in this investigation are now available to support this assertion.

Acknowledgment. We are grateful for support of this work at the University of Illinois from the National Institutes of Health through Grant HL 13652 to D.N.H.

Supplementary Material Available: Figures 1S (disorder models for C₃F₇ in **2**), 2S (μ_{eff} temperature plot for **1** and **3**), 3S (powder diffraction patterns for **1** and **4**), 4S (stereopacking diagram of **1**), 5S (stereopacking diagram of **2**), and 6S (drawing of **5** and projection of unit cell contents) and Tables IIS (anisotropic thermal parameters for **1**), IIIS (anisotropic thermal parameters for **2**), IVS (bond distances and angles involving hydrogen in **1**), VS (bond distances and angles involving the C₃F₇ substituents in **2**), VIS1 (least-squares planes in **1**), VIS2 (least-squares planes in **2**), and VIIS (observed and calculated magnetic susceptibility data for **1–3**, **5**) (17 pages); structure factor listings for **1** and **2** (29 pages). Ordering information is given on any current masthead page.

(92) Girerd, J. J.; Jeannin, S.; Jeannin, Y.; Kahn, O. *Inorg. Chem.* **1978**, *17*, 3034–3040.

(93) Veit, R.; Girerd, J. J.; Kahn, O.; Robert, F.; Jeannin, Y.; El Murr, N. *Inorg. Chem.* **1984**, *23*, 4448–4454.

(94) Chiari, B.; Helms, J. H.; Piovesana, O.; Tarantelli, T.; Zanazzi, P. F. *Inorg. Chem.* **1986**, *25*, 870–874.

(95) Felthouse, T. R.; Hendrickson, D. N. *Inorg. Chem.* **1978**, *17*, 2636–2648.